Structure-preserving reduced order model for parametric cross-diffusion systems

Jad Dabaghi, Virginie Ehrlacher

Structure-preserving reduced order model for parametric cross-diffusion systems *

Jad Dabaghi † Virginie Ehrlacher †

June 15, 2022

Abstract

In this work, we construct a structure-preserving reduced-order model for the resolution of parametric cross-diffusion systems. Cross-diffusion systems model the evolution of the concentrations or volumic fractions of mixtures composed of different species and often read as nonlinear degenerated parabolic partial differential equations whose numerical resolutions are highly expensive from a computational point of view. We are interested here in cross-diffusion systems which exhibit a so-called entropic structure, in the sense that they can be formally written as gradient flows of a certain entropy functional which is actually a Lyapunov functional of the system. In this work, we propose a new reduced-order modelling method, based on a reduced basis paradigm, in order to accelerate the resolution of parameter-dependent cross-diffusion systems, which preserves, at the level of the reduced-order model, the main mathematical properties of the continuous solution, namely mass conservation, non-negativeness, preservation of the volume-filling property and entropy-entropy dissipation relationship. The theoretical advantages of our approach are confirmed by several numerical experiments.

Résumé

Dans ce travail, nous construisons un modèle réduit préservant la structure lors de la résolution d'un système de diffusion croisée. Les systèmes de diffusion croisée modélisent l'évolution des concentrations ou fractions volumiques locales de différentes espèces chimiques constituant un mélange et s'interprètent souvent comme des systèmes d'équations aux dérivées partielles non linéaires dégénérées dont la résolution numérique est très coûteuse. Nous nous intéressons dans ce travail à des systèmes de diffusion croisée ayant une structure entropique, dans le sens où ils peuvent s'écrire comment le flot de gradient d'une certaine fonctionnelle d'entropie; cette dernière étant une fonction de Lyapunov pour ce système. Dans ce travail, nous proposons une nouvelle méthode de réduction de modèle, basée sur une approche de type base réduite, afin d'accélérer la résolution de systèmes de diffusion croisée dépendant de paramètres. Cette résolution préserve au niveau réduit les principales propriétés mathématiques imposées par la solution au niveau continu à savoir la conservation de la masse, la positivité de la solution, la contrainte de volume, et la dissipation d'entropie. Les essais numériques confirmes les avantages de notre approche.

keywords: cross-diffusion systems, finite volumes, Proper orthogonal decomposition.

1 Introduction

The study of cross-diffusion systems for the modeling of diffusive phenomena with multi-component mixtures has received a steadily growing amount of attention from mathematicians in the last decade. These systems arise in various application fields such as population dynamics [31] or growth of vascular tumors in medical biology [15]. In chemistry, such systems are used in order to model the evolution of densities, concentrations or volumic fractions of the various chemical species composing the mixture of interest [1]. Despite their practical relevance in a wide range of application fields, significant steps in their mathematical understanding have only been achieved recently. This is due to the fact that these systems usually read as coupled degenerate nonlinear systems, for which traditional analysis tools do not apply. It has been

*This project has received funding from the ANR project "COMODO" (ANR-19-CE46-0002).

†CERMICS, Ecole des Ponts, 77455 Marne-la-Vallée cedex 2

recently understood [4, 16] that such systems can be formally seen as gradient flows of a certain entropy functional with respect to a metric which can be seen as an extension of the so-called Wasserstein metric. As a consequence, the corresponding entropy functional can be seen as a Lyapunov function for the cross-diffusion system. The rate of decay of the entropy functional can then give precious insight on the long-time behaviour of the solutions of the cross-diffusion system.

The development of numerical methods for the resolution of such systems has been a very active field of research in the recent years. The challenges there are to design numerical schemes which preserve the main mathematical properties of the continuous model at the discrete level such as non-negativity of the solutions and entropy-entropy dissipation relationship. Finite element schemes have been proposed for instance in [2], while structure-preserving finite-volume schemes have been studied in [6, 18]. The resolution of such schemes, which is usually based on implicit numerical schemes for nonlinear models, remains quite costly from a computational point of view especially when the number of species in the system or the number of spatial degrees of freedom is large.

The complexity of these computations becomes prohibitive when the cross-diffusion model depends on some parameters since it is necessary to compute the solution of these systems for many values of these parameters. The resolution of inverse problems so as to identify optimal values of these parameters which enable to reproduce experimental results is an example of such a context, where a significant parametric study has to be performed. As an alternative, model-order reduction techniques have been developed for many type of problems so as to alleviate the computational burden of parametric studies. Reduced order model techniques have been proved to yield computationally effective approaches to approximate the solution of parametrized partial differential equations encountered in many problems in science and engineering [14, 29]. Several methods have been developed in the literature. Among them we mention the Proper Orthogonal Decomposition (POD) method [12, 3, 22, 23, 13, 11], the Proper Generalized Decomposition (PGD) method [27, 24, 21] or reduced basis methods [26, 25, 14, 29].

The aim of the present work is to develop a new structure-preserving reduced-order model, relying on a POD/Reduced Basis paradigm, so as to compute the solution of parametrized cross-diffusion equations which exhibit an entropic structure. Indeed, the reduced-order model we propose here preserves the main theoretical features of the continuous cross-diffusion model, namely non-negativity of the solutions, mass conservation and entropy-entropy dissipation relationship, whereas a standard POD reduced-order model does not.

Our paper is organized as follows. In Section 2, we present the cross-diffusion model and its mathematical properties. In particular, in Section 2.2 we present the cell-centered finite volume method preserving the structural properties of the solution proposed in [5]. The finite-volume scheme is the high-fidelity solver we consider in this work. Section 3 is dedicated to the construction of the structure-preserving reduced model and its properties. Finally, in Section 4 we present numerical experiments showing the advantages of our approach.

2 Parametric cross-diffusion system

The aim of this section is to introduce the parametric cross-diffusion system considered in this work, together with the main mathematical properties of the solution which we wish to be preserved by any reduced-order model. We also describe here the discrete numerical scheme used in order to perform high-fidelity computations.

2.1 Continuous model and main mathematical properties

Let $\Omega \subset \mathbb{R}^d$, $d > 1$, be a polygonal domain, let $\boldsymbol{n}$ denote its outward unit normal vector, and let $T > 0$ be the final simulation time. We consider a diffusive mixture of $N_\mathrm{s} \in \mathbb{N}^*$, $N_\mathrm{s} \geq 2$, chemical species, and assume that the diffusion laws of the different species within the mixture are parametrized by a vector of parameters $\mu \in \mathbb{R}^p$ for some $p \in \mathbb{N}^*$ and belonging to a set of parameter values $\mathcal{P} \subset \mathbb{R}^p$. For all $t \in [0,T]$, $x \in \Omega$ and $1 \leq i \leq N_\mathrm{s}$, we denote by $u_{\mu,i}(t,x)$ the value of the local volumic fraction of species $1 \leq i \leq N_\mathrm{s}$ at time $t \in [0,T]$, point $x \in \Omega$ and parameter value $\mu \in \mathcal{P}$. We also denote by $\boldsymbol{u}_\mu := (u_{\mu,1}, \ldots, u_{\mu,N_\mathrm{s}})$ the set of all N_s volumic fractions.

We assume that the evolution of $\boldsymbol{u}_\mu$ is ruled by a parametrized cross-diffusion model with no-flux boundary conditions of the following form for all $\mu \in \mathcal{P}$:

$$\begin{aligned} \partial_t u_{\mu,i} - \boldsymbol{\nabla} \cdot \left(\sum_{j=1}^{N_\mathrm{s}} \mathbb{A}_{\mu,ij}(\boldsymbol{u}_\mu) \boldsymbol{\nabla} u_{\mu,j} \right) = 0, \quad \text{in } \Omega \times [0,T], \quad \forall i \in [\![1, N_\mathrm{s}]\!], \\ \left(\sum_{j=1}^{N_\mathrm{s}} \mathbb{A}_{\mu,ij}(\boldsymbol{u}_\mu) \boldsymbol{\nabla} u_{\mu,j} \right) \cdot \boldsymbol{n} = 0, \quad \text{in } \partial\Omega \times [0,T], \quad \forall i \in [\![1, N_\mathrm{s}]\!], \\ u_{\mu,i}(\boldsymbol{x}, 0) = u_i^0(\boldsymbol{x}), \quad \text{in } \Omega, \quad \forall i \in [\![1, N_\mathrm{s}]\!], \end{aligned} \tag{2.1}$$

for some initial conditions $(u_1^0, \cdots, u_{N_\mathrm{s}}^0) \in [L^\infty(\Omega)]^{N_\mathrm{s}}$, and where for all $1 \leq i, j \leq N_\mathrm{s}$, $\mathbb{A}_{\mu,ij} : \mathbb{R}^{N_\mathrm{s}} \to \mathbb{R}$ is a smooth cross-diffusion coefficient.

The aim of our work is to propose a structure-preserving reduced order model for the resolution of parametrized cross-diffusion systems of the form (2.1) which have additional physically relevant mathematical properties, more precisely which

- (i) preserves mass conservation,
- (ii) preserves the non-negativeness of solutions,
- (iii) satisfy volume-filling constraints,
- (iv) preserves the entropic structure of the cross-diffusion system.

We explain in more details these four properties below.

For the sake of simplicity, we will consider in the following one particular type of parametrized cross-diffusion which satisfy these properties, and explain the strategy we propose for building a structure preserving reduced order model on this particular system. However, we would like to emphasize the fact that the approach proposed here can be easily adapted to other types of cross-diffusion systems enjoying similar mathematical properties.

From now on, let us assume that

$$\mathcal{P} := \left\{ \mu := (a_{ij})_{1 \leq i \neq j \leq N_\mathrm{s}} \in (\mathbb{R}_+^*)^{N_\mathrm{s}(N_\mathrm{s}-1)}, \;\; a_{ij} = a_{ji} \quad \forall 1 \leq i \neq j \leq N_\mathrm{s} \quad \right\}.$$

and that for all $\mu := (a_{ij})_{1 \leq i \neq j \leq N_\mathrm{s}} \in \mathcal{P}$, all $\boldsymbol{u} := (u_1, \cdots, u_{N_\mathrm{s}}) \in \mathbb{R}^{N_\mathrm{s}}$ and all $1 \leq i \neq j \leq N_\mathrm{s}$,

$$\mathbb{A}_{\mu,ii}(\boldsymbol{u}) = \sum_{j=1, j \neq i}^{N_\mathrm{s}} a_{ij} u_j, \qquad \text{and} \qquad \mathbb{A}_{\mu,ij}(\boldsymbol{u}) = -a_{ij} u_i.$$

Then, system (2.1) boils down to:

$$\begin{aligned} \partial_t u_{\mu,i} - \boldsymbol{\nabla} \cdot \left(\sum_{1 \leq j \neq i \leq N_\mathrm{s}} a_{ij} \left(u_{\mu,j} \boldsymbol{\nabla} u_{\mu,i} - u_{\mu,i} \boldsymbol{\nabla} u_{\mu,j} \right) \right) = 0 \quad \text{in} \quad \Omega \times [0,T], \text{ for } i \in [\![1, N_\mathrm{s}]\!], \\ \left(\sum_{1 \leq j \neq i \leq N_\mathrm{s}} a_{ij} \left(u_{\mu,j} \boldsymbol{\nabla} u_{\mu,i} - u_{\mu,i} \boldsymbol{\nabla} u_{\mu,j} \right) \right) \cdot \boldsymbol{n} = 0 \quad \text{on} \quad \partial\Omega \times [0,T], \text{ for } i \in [\![1, N_\mathrm{s}]\!], \\ u_{\mu,i}(\boldsymbol{x}, 0) = u_i^0(\boldsymbol{x}) \quad \text{in} \quad \Omega, \text{ for } i \in [\![1, N_\mathrm{s}]\!]. \end{aligned} \tag{2.2}$$

This system has been originally introduced in [32, 1]. It is used in particular in [1] in order to model diffusion phenomena in the bulk of a thin-film layer solar cell during its production process by physical vapor deposition. Since for all $\mu \in \mathcal{P}$ and all $1 \leq i \leq N_\mathrm{s}$, $u_{\mu,i}(t,x)$ represents the local volumic fraction of specie i at time t and point $x \in \Omega$, it is expected from a physical point of view that each function $u_{\mu,i}$

to be non-negative and to satisfy the so-called *volumic constraint* which reads as $\sum_{i=1}^{N_s} u_{\mu,i}(t,x) = 1$ for all $(t,x) \in (0,T)\times\Omega$.

This is the reason why we introduce the set $\mathcal{A} \subset \mathbb{R}^{N_s}$, which is defined by

$$\mathcal{A} := \left\{ \boldsymbol{u} = (u_1, \cdots, u_{N_s}) \in \mathbb{R}_+^{N_s},\ \sum_{i=1}^{N_s} u_i = 1 \right\}.$$

From now on, let us assume that the initial condition $\boldsymbol{u}^0 := (u_1^0, \cdots, u_{N_s}^0)$ satisfies $\boldsymbol{u}^0(x) \in \mathcal{A}$ for almost all $x \in \Omega$. Let us assume in addition that

$$\int_\Omega u_i^0(x)\,\mathrm{d}x > 0, \quad \forall i \in [\![1, N_s]\!].$$

Then, it is proved in [1] that there exists at least one weak solution $\boldsymbol{u}_\mu \in L^2((0,T), H^1(\Omega))^{N_s}$ such that $\partial_t \boldsymbol{u}_\mu \in L^2((0,T), H^1(\Omega)')^{N_s}$ to system (2.2). Moreover, such a weak solution can be proved to satisfy the following properties:

(P1) **mass conservation:** for all $t \in [0,T]$ and all $1 \le i \le N_s$, $\int_\Omega u_{\mu,i}(t,x)\,\mathrm{d}x = \int_\Omega u_i^0(x)\,\mathrm{d}x$.

(P2) **volume-filling constraint:** $\boldsymbol{u}_\mu(t,x) \in \mathcal{A}$ for almost all $(t,x) \in (0,T)\times\Omega$.

Moreover, system (2.2) has a formal gradient flow structure, which we make more precise below, which implies that such a weak solution satisfies an entropy-entropy dissipation inequality. We introduce the entropy functional $E : L^\infty(\Omega, \mathcal{A}) \to \mathbb{R}$ defined by

$$\forall \boldsymbol{u} := (u_i)_{1\le i\le N_s} \in L^\infty(\Omega, \mathcal{A}), \quad E(\boldsymbol{u}) := \int_\Omega \left(\sum_{i=1}^{N_s} u_i(t,x) \ln(u_i(t,x)) \right) \mathrm{d}x. \tag{2.3}$$

Following [1, Section 1.1.2] and [6, Proposition 1.3], it holds that system (2.2) enjoys a formal gradient flow structure and that the functional E is a Lyapunov function. More precisely, the following entropy-entropy dissipation inequality holds for all $\mu := (a_{ij})_{1\le i\ne j\le N_s} \in \mathcal{P}$: for almost all $t \in (0,T)$,

$$\frac{d}{dt} E(\boldsymbol{u}_\mu(t,\cdot)) + \int_\Omega \left(\sum_{1\le i<j\le N_s} a_{ij} u_{\mu,i}(t,x) u_{\mu,j}(t,x) |\boldsymbol{\nabla} \ln(u_{\mu,i}(t,x)) - \boldsymbol{\nabla} \ln(u_{\mu,j}(t,x))|^2 \right) \mathrm{d}x = 0.$$

Denoting by

$$a_\mu^\star := \min_{1\le i\ne j\le N_s} a_{ij}, \tag{2.4}$$

it can be shown that

$$\begin{aligned}\int_\Omega \left(\sum_{1\le i<j\le N_s} a_{ij} u_{\mu,i}(t,x) u_{\mu,j}(t,x) |\boldsymbol{\nabla} \ln(u_{\mu,i}(t,x)) - \boldsymbol{\nabla} \ln(u_{\mu,j}(t,x))|^2 \right) \mathrm{d}x &\ge a_\mu^\star \sum_{i=1}^{N_s} \int_\Omega |\boldsymbol{\nabla} \sqrt{u_{\mu,i}}(t,x)|^2\,\mathrm{d}x \\ &= a_\mu^\star \sum_{i=1}^{N_s} \int_\Omega u_{\mu,i}(t,x) |\boldsymbol{\nabla} \ln(u_{\mu,i})(t,x)|^2\,\mathrm{d}x,\end{aligned}$$

which implies that system (2.2) satisfies the following entropy-entropy dissipation relation.

(P3) **Entropy-entropy dissipation relation:** for almost all $t \in (0,T)$,

$$\frac{d}{dt} E(\boldsymbol{u}_\mu(t,\cdot)) + a_\mu^\star \sum_{i=1}^{N_s} \int_\Omega u_{\mu,i}(t,x) |\boldsymbol{\nabla} \ln(u_{\mu,i}(t,x))|^2\,\mathrm{d}x \le 0.$$

Remark 2.1. *Other types of cross-diffusion systems enjoy similar mathematical properties as the ones highlighted here for system (2.2). The Maxwell-Stefan [17, 5] cross-diffusion model is another example of system for which the reduced order modeling strategy we propose here can be easily adapted.*

In the following section, we describe the finite volume numerical scheme we use here in order to compute high-fidelity solutions of system (2.2) and summarize its main mathematical properties. This finite volume scheme, which was introduced in [6], actually preserves analogous versions of properties (P1)-(P2)-(P3) on the discrete level.

2.2 High-fidelity discretization: structure-preserving finite-volume scheme

2.2.1 Definition of the scheme and notation

For the time discretization, we introduce a division of the interval $[0,T]$ into subintervals $I_n := [t_{n-1}, t_n]$, $1 \leq n \leq N_t$, such that $0 = t_0 < t_1 < \cdots < t_{N_t} = T$. The time steps are denoted by $\Delta t_n = t_n - t_{n-1}$, $n = 1, \cdots, N_t$.

For the space discretization, we consider an admissible mesh of Ω in the sense of [6, Definition 2.1](see also [10]). We recall this definition here for the sake of completeness.

Definition 2.2. *An admissible mesh of Ω is a triplet $(\mathcal{T}_h, \mathcal{E}_h, (x_K)_{K\in\mathcal{T}_h})$ such that the following conditions are fulfilled.*

- *Each control volume (or cell) $K \in \mathcal{T}_h$ is non-empty, open, polyhedral and convex. We assume that $K \cap L = \emptyset$ if $K, L \in \mathcal{T}_h$ with $K \neq L$, while $\bigcup_{K\in\mathcal{T}_h} \overline{K} = \overline{\Omega}$. We denote by m_K the d-dimensional Lebesgue measure of the cell K.*
- *Each face $\sigma \in \mathcal{E}_h$ is closed and is contained in a hyperplane of $\mathbb{R}^d$, with positive $(d-1)$-dimensional Hausdorff (or Lebesgue) measure denoted by $m_\sigma := \mathcal{H}^{d-1}(\sigma) > 0$. We assume that $\mathcal{H}^{d-1}(\sigma \cap \sigma') = 0$ for $\sigma, \sigma' \in \mathcal{E}_h$ unless $\sigma' = \sigma$. For all $K \in \mathcal{T}_h$, we assume that there exists a subset $\mathcal{E}_h^K$ of $\mathcal{E}_h$ such that $\partial K = \bigcup_{\sigma\in\mathcal{E}_h^K} \sigma$. Moreover, we suppose that $\bigcup_{K\in\mathcal{T}_h} \mathcal{E}_h^K = \mathcal{E}_h$. Given two distinct cells $K, L \in \mathcal{T}_h$, the intersection $K \cap L$ either reduces to a single face $\sigma \in \mathcal{E}_h$ denoted by $K|L$, or its $(d-1)$-dimensional Hausdorff measure is 0.*
- *The cell-centers $(x_K)_{K\in\mathcal{T}_h}$ satisfy $x_K \in K$, and are such that, if $K, L \in \mathcal{T}_h$ share a face $K|L$, then the vector $x_L - x_K$ is orthogonal to $K|L$.*
- *For the boundary faces $\sigma \in \partial\Omega$ with $\sigma \in \mathcal{E}_K$ for some $K \in \mathcal{T}_h$, we assume additionally that there exists $x_\sigma \in \sigma$ such that $x_\sigma - x_K$ is orthogonal to σ. We denote by $\mathcal{E}_h^{\rm ext}$ the set of boundary faces, i.e. the set of faces $\sigma \in \mathcal{E}_h$ such that $\sigma \subset \partial\Omega$ and by $\mathcal{E}_h^{\rm int} := \mathcal{E}_h \setminus \mathcal{E}_h^{\rm ext}$ the set of interior faces.*

Denote by h_K the diameter of the generic element $K \in \mathcal{T}_h$ and $h := \max_{K\in\mathcal{T}_h} h_K$. The number of elements in the mesh $\mathcal{T}_h$ is denoted by N_h. Given a vector $\boldsymbol{c} := (c_K)_{K\in\mathcal{T}_h} \in \mathbb{R}^{N_h}$, we define for all $K \in \mathcal{T}_h$ and face $\sigma \in \mathcal{E}_h^K$, the mirror value $c_{K\sigma}$ of c_K across σ by setting:

$$c_{K\sigma} := c_L \quad \text{if} \quad \sigma = K|L \in \mathcal{E}_h^{\rm int} \quad \text{and} \quad c_{K\sigma} := c_K \quad \text{if} \quad \sigma \in \mathcal{E}_h^{\rm ext}. \tag{2.5}$$

We also define the oriented and absolute jumps of $\boldsymbol{c} \in \mathbb{R}^{N_h}$ across any edge by

$$D_{K\sigma}\boldsymbol{c} := c_{K\sigma} - c_K, \quad \text{and} \quad D_\sigma \boldsymbol{c} := |D_{K\sigma}\boldsymbol{c}|, \quad \forall K \in \mathcal{T}_h,\ \forall \sigma \in \mathcal{E}_h^K. \tag{2.6}$$

Remark 2.3. *For all $K \in \mathcal{T}_h$ and all $\sigma \in \mathcal{E}_h^K \cap \mathcal{E}_h^{\rm int}$ such that $\sigma = K|L$,*

$$D_{L\sigma}\boldsymbol{c} = c_{L\sigma} - c_L = c_K - c_L = -D_{K\sigma}\boldsymbol{c}. \tag{2.7}$$

Given $\sigma \in \mathcal{E}_h$, we define by

$$d_\sigma := \begin{cases} |x_K - x_L| & \text{if } \sigma = K|L \in \mathcal{E}_h^{\rm int}, \\ |x_K - x_\sigma| & \text{if } \sigma \in \mathcal{E}_h^K \cap \mathcal{E}_h^{\rm ext}, \end{cases} \qquad \text{and} \qquad \tau_\sigma := \frac{m_\sigma}{d_\sigma}.$$

Let $\mu \in \mathcal{P}$. Using the cell-centered finite volume method introduced in [6], the unknown of the model (2.2) is discretized using a couple of constant values per cell: for all $1 \le n \le N_t$, we let

$$\boldsymbol{U}_\mu^n := \left(u_{\mu,i,K}^n\right)_{K\in\mathcal{T}_h, i\in[1,N_{\rm s}]} \in \mathbb{R}^{N_h\times N_{\rm s}},$$

where $u_{\mu,i,K}^n$ is a numerical approximation of $\dfrac{1}{m_K}\displaystyle\int_K u_{\mu,i}(t_n,x)\,dx$.

The finite volume scheme we use is then the following: for $\boldsymbol{U}^0 := \left(u_{i,K}^0\right)_{K\in\mathcal{T}_h, i\in[1,N_{\rm s}]} \in \mathbb{R}^{N_h\times N_{\rm s}}$ given, where $u_{i,K}^0 = \dfrac{1}{m_K}\displaystyle\int_K u_i^0(x)\,{\rm d}x$, for all $1 \le n \le N_t$, we find $\boldsymbol{U}_\mu^n \in \mathbb{R}^{N_h\times N_{\rm s}}$ satisfying

$$m_K \frac{u_{\mu,i,K}^n - u_{\mu,i,K}^{n-1}}{\Delta t_n} + \sum_{\sigma\in\mathcal{E}_h^K} F_{\mu,i,K\sigma}(\boldsymbol{U}_\mu^n) = 0, \quad \forall K \in \mathcal{T}_h,\ \forall i \in [1,N_{\rm s}] \tag{2.8}$$

where for all $\boldsymbol{U} := (u_{i,K})_{1\le i\le N_{\rm s}, K\in\mathcal{T}_h} \in \mathbb{R}^{N_h\times N_{\rm s}}$, we will denote by

$$F_{\mu,i,K\sigma}(\boldsymbol{U}) := \begin{cases} -a_\mu^\star \tau_\sigma D_{K\sigma}\boldsymbol{u}_i - \tau_\sigma \left(\sum_{j=1,\, j\neq i}^{N_{\rm s}} \left(a_{ij} - a_\mu^\star\right)\left(u_{j,\sigma} D_{K\sigma}\boldsymbol{u}_i - u_{i,\sigma} D_{K\sigma}\boldsymbol{u}_j\right)\right) & \text{if } \sigma \in \mathcal{E}_h^{\rm int}, \\ 0 & \text{if } \sigma \in \mathcal{E}_h^{\rm ext}, \end{cases} \tag{2.9}$$

where

$$u_{i,\sigma} := \begin{cases} 0 & \text{if } \min(u_{i,K}, u_{i,K\sigma}) < 0, \\ u_{i,K} & \text{if } u_{i,K} = u_{i,K\sigma} \ge 0, \\ \dfrac{u_{i,K} - u_{i,K\sigma}}{\ln(u_{i,K}) - \ln(u_{i,K\sigma})} & \text{otherwise.} \end{cases} \tag{2.10}$$

Remark 2.4. *Observe that the numerical flux defined in (2.9) is conservative in the sense that for $\sigma \in \mathcal{E}_h^{\rm int}$, $\sigma = K|L$, and all $\boldsymbol{U} \in \mathbb{R}^{N_h\times N_{\rm s}}$,*

$$F_{\mu,i,L\sigma}(\boldsymbol{U}) = -F_{\mu,i,K\sigma}(\boldsymbol{U}).$$

This implies in particular that, for all $1 \le i \le N_{\rm s}$

$$\sum_{K\in\mathcal{T}_h} \sum_{\sigma\in\mathcal{E}_h^K\cap\mathcal{E}_h^{\rm int}} F_{\mu,i,K\sigma}(\boldsymbol{U}_\mu^n) = 0. \tag{2.11}$$

2.2.2 Properties of the discrete solution

It is proved in [6] that the numerical scheme defined in the previous section is well-defined and preserves analogous properties as (P1)-(P2)-(P3) at the discrete level. These properties are collected in Proposition 2.5 below.

Proposition 2.5 (Theorem 2.2 of [6]). *Let $\boldsymbol{u}^0 \in L^\infty(\Omega;\mathcal{A})$ so that $\boldsymbol{U}^0 \in \mathbb{R}^{N_h\times N_{\rm s}}$ is defined as $u_{i,K}^0 = \dfrac{1}{m_K}\displaystyle\int_K u_i^0(x)\,{\rm d}x$. Then, for all $1 \le n \le N_t$, there exists at least one solution $\boldsymbol{U}_\mu^n \in \mathbb{R}^{N_h\times N_{\rm s}}$ to the numerical scheme (2.8) which satisfies the following properties:*

*($P1^h$) **mass conservation:***

$$\sum_{K\in\mathcal{T}_h} m_K u_{\mu,i,K}^n = \sum_{K\in\mathcal{T}_h} m_K u_{\mu,i,K}^0 = \int_\Omega u_i^0(x)\,{\rm d}x \quad \forall i \in [\![1,N_{\rm s}]\!], \quad \forall n \in [\![0,N_t]\!]. \tag{2.12}$$

($P2^h$) ***volume-filling constraint:***

$$u^n_{\mu,i,K} > 0 \quad \forall K \in \mathcal{T}_h, \quad \forall i \in [\![1, N_s]\!], \quad \forall n \in [\![0, N_t]\!], \tag{2.13}$$

and

$$\sum_{i=1}^{N_s} u^n_{\mu,i,K} = 1 \quad \forall K \in \mathcal{T}_h, \quad \forall n \in [\![0, N_t]\!]. \tag{2.14}$$

($P3^h$) ***entropy-entropy dissipation inequality:*** *For all $\boldsymbol{U} := (u_{i,K})_{K\in\mathcal{T}_h, 1\le i\le N_s} \in (\mathbb{R}_+)^{N_h\times N_s}$, let us define*

$$E_{\mathcal{T}_h}(\boldsymbol{U}) := \sum_{K\in\mathcal{T}_h}\sum_{i=1}^{N_s} m_K u_{i,K}\ln(u_{i,K}). \tag{2.15}$$

Then, it holds that

$$\frac{1}{\Delta t_n}(E_{\mathcal{T}_h}(\boldsymbol{U}^n_\mu) - E_{\mathcal{T}_h}(\boldsymbol{U}^{n-1}_\mu)) + a^\star_\mu \sum_{\sigma\in\mathcal{E}_h}\sum_{i=1}^{N_s} u^n_{\mu,i,\sigma}|D_{K\sigma}\ln(\boldsymbol{u}^n_{\mu,i})|^2 \le 0, \quad \forall n \in [\![1, N_t]\!]. \tag{2.16}$$

2.2.3 Newton resolution

Let us define for all $\mu \in \mathcal{P}$, $\forall K \in \mathcal{T}_h$, $\forall i \in [\![1, N_s]\!]$, $\forall 1 \le n \le N_t$, the nonlinear function $G^n_{\mu,i,K} : \mathbb{R}^{N_s\times N_h} \to \mathbb{R}$ defined as follows: for all $\boldsymbol{U} = (u_{i,K})_{1\le i\le N_s, K\in\mathcal{T}_h} \in \mathbb{R}^{N_h\times N_s}$,

$$G^n_{\mu,i,K}(\boldsymbol{U}) := m_K\frac{u_{i,K} - u^{n-1}_{\mu,i,K}}{\Delta t_n} + \sum_{\sigma\in\mathcal{E}^K_h\cap\mathcal{E}^{\rm int}_h} F_{\mu,i,K\sigma}(\boldsymbol{U}), \tag{2.17}$$

and define the application $G^n_\mu : \mathbb{R}^{N_s\times N_h} \to \mathbb{R}^{N_s\times N_h}$ as follows: for all $\boldsymbol{U} \in \mathbb{R}^{N_s\times N_h}$,

$$G^n_\mu(\boldsymbol{U}) := \left(G^n_{\mu,i,K}(\boldsymbol{U})\right)_{K\in\mathcal{T}_h, 1\le i\le N_s}.$$

A solution $\boldsymbol{U}^n_\mu \in \mathbb{R}^{N_h\times N_s}$ to the scheme (2.8) can then be rewritten equivalently as a solution to

$$G^n_\mu(\boldsymbol{U}^n_\mu) = 0, \tag{2.18}$$

which we solve in practice using a classical Newton procedure [20].

The resolution of problem (2.18) can be very expensive due to the number of mesh elements, the number of species, the number of time steps, and the number of cross diffusion matrix to be tested. It is then crucial to speed up the computation of the numerical solution. The aim of our work is to propose a new reduced-order model to efficiently compute approximations of $\boldsymbol{U}^n_\mu$ for a large number of values of $\mu \in \mathcal{P}$ while preserving analogous properties as those listed in Lemma 2.5.

3 Structure-preserving reduced-order model

In Section 3.2, we expose the structure-preserving reduced-order model we propose in order to efficiently compute numerical approximations of $\boldsymbol{U}^n_\mu$ for $1 \le n \le N_t$ and $\mu \in \mathcal{P}$. For the sake of comparison, we first describe how a standard reduced-order modeling method based on a POD approach would work in Section 3.1. We will compare the two approaches in our numerical experiments presented in Section 4.

In the following, we introduce $\mathcal{P}_{\rm train} \subset \mathcal{P}$ a finite training set of parameter values, and assume that we have computed high-fidelity solutions $\left(\boldsymbol{U}^n_\mu\right)_{1\le n\le N_t}$ for all values of the parameter μ in the training set $\mathcal{P}_{\rm train}$ according the finite volume scheme described in Section 2.2. We will denote by $p \in \mathbb{N}^*$ the cardinality of the set $\mathcal{P}_{\rm train}$.

3.1 Standard POD reduced model

The aim of this section is to describe the classical POD reduced-order model (POD-ROM) we will use in our numerical experiments to compare with the structure-preserving reduced-order model (SP-ROM) we will introduce in Section 3.2.

Given the family of snapshot solutions $\left(\boldsymbol{U}_\mu^n\right)_{1\leq n\leq N_t,\mu\in\mathcal{P}_{\text{train}}} \in \mathbb{R}^{N_h\times N_s}$, for all $r\in\mathbb{N}^*$, we denote by $\boldsymbol{V}^1,\cdots,\boldsymbol{V}^r\in\mathbb{R}^{N_h\times N_s}$ the r first POD modes of this family.

In the classical POD-ROM, for all $\mu\in\mathcal{P}$ and $1\leq n\leq N_t$, we compute a reduced-order model approximation $\widetilde{\boldsymbol{U}}_\mu^n\in\mathbb{R}^{N_s\times N_h}$ of $\boldsymbol{U}_\mu^n$ as a linear combination of $\boldsymbol{V}^1,\cdots,\boldsymbol{V}^r$

$$\widetilde{\boldsymbol{U}}_\mu^n := \sum_{k=1}^r c_\mu^{k,n}\boldsymbol{V}^k, \tag{3.1}$$

where the coefficients $\boldsymbol{c}_\mu^n := (c_\mu^{k,n})_{1\leq k\leq r}\in\mathbb{R}^r$ are computed as follows.

Let us denote by $(V_{i,K}^k)_{K\in\mathcal{T}_h,1\leq i\leq N_s}\in\mathbb{R}^{N_h\times N_s}$ the components of $\boldsymbol{V}^k$ for all $1\leq k\leq r$. For any vector $\boldsymbol{c}:=(c^k)_{1\leq k\leq r}\in\mathbb{R}^r$, let us denote by $\widetilde{\boldsymbol{U}}(\boldsymbol{c}) := (\widetilde{u}_{i,K}(\boldsymbol{c}))_{K\in\mathcal{T}_h,1\leq i\leq N_s}\in\mathbb{R}^{N_h\times N_s}$ the vector defined so that

$$\widetilde{u}_{i,K}(\boldsymbol{c}) := \sum_{k=1}^r c^k V_{i,K}^k \quad \forall i\in[\![1,N_s]\!], \quad \forall K\in\mathcal{T}_h. \tag{3.2}$$

Let us now define for all $\mu\in\mathcal{P}$, $1\leq n\leq N_t$, $1\leq i\leq N_s$ and $K\in\mathcal{T}_h$, the application $\widetilde{G}_{\mu,i,K}^n:\mathbb{R}^r\to\mathbb{R}$ defined by

$$\widetilde{G}_{\mu,i,K}^n(\boldsymbol{c}) := m_K\frac{\widetilde{u}_{i,K}(\boldsymbol{c})-\widetilde{u}_{\mu,i,K}^{n-1}}{\Delta t_n} + \sum_{\sigma\in\mathcal{E}_h^K} F_{\mu,i,K\sigma}\left(\widetilde{\boldsymbol{U}}(\boldsymbol{c})\right),$$

where $\widetilde{u}_{\mu,i,K}^0(\boldsymbol{c}) := u_{i,K}^0$, and by $\widetilde{G}_\mu^n(\boldsymbol{c}) := \left(\widetilde{G}_{\mu,i,K}^n(\boldsymbol{c})\right)_{K\in\mathcal{T}_h,1\leq i\leq N_s}$. Let us finally denote by $\widetilde{H}_\mu^n:\mathbb{R}^r\to\mathbb{R}^r$ the application such that, for all $\boldsymbol{c}\in\mathbb{R}^r$, $\widetilde{H}_\mu^n = \left(\widetilde{H}_\mu^{n,l}(\boldsymbol{c})\right)_{1\leq l\leq r}$ where for all $1\leq l\leq r$,

$$\widetilde{H}_\mu^{n,l}(\boldsymbol{c}) := \left\langle \boldsymbol{V}^l, \widetilde{G}_\mu^n(\boldsymbol{c})\right\rangle,$$

where $\langle\cdot,\cdot\rangle$ denotes the euclidean scalar product of $\mathbb{R}^{N_h\times N_s}$. Then, the vector $\boldsymbol{c}_\mu^n\in\mathbb{R}^r$ is defined as a solution to

$$\widetilde{H}_\mu^n(\boldsymbol{c}_\mu^n) = 0, \tag{3.3}$$

and the numerical approximation $\widetilde{\boldsymbol{U}}_\mu^n$ of $\boldsymbol{U}_\mu^n$ given by the classical POD-ROM is given by ((3.1)). A solution to problem (3.3) is computed using a classical Newton algorithm.

Let us highlight here that the standard POD reduced-order model may not preserve the structural properties of the solutions of the cross-diffusion system we mentioned in the previous sections, such as non-negativeness, mass conservation, volumic constraint and decay of the entropy with respect to time evolution.

3.2 Structure-preserving (SP) reduced-order model

For all $\mu\in\mathcal{P}$, $1\leq i\leq N_s$, $0\leq n\leq N_t$ and $K\in\mathcal{T}_h$, let us denote by $z_{\mu,i,K}^n := \ln(u_{\mu,i,K}^n)$ and by $\boldsymbol{Z}_\mu^n := \left(z_{\mu,i,K}^n\right)_{K\in\mathcal{T}_h,1\leq i\leq N_s}\in\mathbb{R}^{N_h\times N_s}$. We then denote by $\boldsymbol{W}^1,\cdots,\boldsymbol{W}^r\in\mathbb{R}^{N_h\times N_s}$ the r first POD modes of the family $\left(\boldsymbol{Z}_\mu^n\right)_{\mu\in\mathcal{P}_{\text{train}},1\leq n\leq N_t}\subset\mathbb{R}^{N_h\times N_s}$. In addition, for all $1\leq i\leq N_s$, we define

$$\boldsymbol{W}^{r+i} := \boldsymbol{I}^i,$$

where $\boldsymbol{I}^i\in\mathbb{R}^{N_s\times N_h}$ is defined by

$$\boldsymbol{I}^i := (I_{j,K}^i)_{K\in\mathcal{T}_h,1\leq j\leq N_s} \quad \text{with} \quad I_{j,K}^i = \delta_j^i. \tag{3.4}$$

In other words, $I^i_{j,K} = 1$ if $i = j$ and 0 otherwise. We also denote by $r_\star := r + N_{\rm s}$.

The principle of the SP-ROM method we present here is to construct for all $\mu \in \mathcal{P}$, a reduced-order model approximation $\overline{\boldsymbol{Z}}^n_\mu \in \mathbb{R}^{N_h \times N_{\rm s}}$ of $\boldsymbol{Z}^n_\mu$ that reads as a linear combination of $\boldsymbol{W}^1, \cdots, \boldsymbol{W}^{r_\star}$ given by

$$\overline{\boldsymbol{Z}}^n_\mu := \sum_{k=1}^{r_\star} c^{k,n}_\mu \boldsymbol{W}^k \tag{3.5}$$

where the vector $\boldsymbol{c}^n_\mu := \left(c^{k,n}_\mu\right)_{1\le k\le r_\star} \in \mathbb{R}^{r_\star}$ is computed as described below. Then, assuming that $\overline{\boldsymbol{Z}}^n_\mu = \left(\overline{z}^n_{\mu,i,K}\right)_{K\in\mathcal{T}_h, 1\le i\le N_{\rm s}}$, a reduced-order model approximation $\overline{\boldsymbol{U}}^n_\mu = \left(\overline{u}^n_{\mu,i,K}\right)_{K\in\mathcal{T}_h, 1\le i\le N_{\rm s}}$ of $\boldsymbol{U}^n_\mu$ is then computed as follows:

$$\overline{u}^n_{\mu,i,K} := \frac{e^{\overline{z}^n_{\mu,i,K}}}{\sum_{j=1}^{N_{\rm s}} e^{\overline{z}^n_{\mu,j,K}}}. \tag{3.6}$$

Note that, by construction, a reduced-order model $\overline{\boldsymbol{U}}^n_\mu$ given under the form (3.6) necessarily satifies

(P2$^{\rm red}$) **volume-filling constraint:**

$$\overline{u}^n_{\mu,i,K} > 0 \quad \forall K \in \mathcal{T}_h, \quad \forall i \in [\![1, N_{\rm s}]\!], \quad \forall n \in [\![0, N_t]\!], \tag{3.7}$$

and

$$\sum_{i=1}^{N_{\rm s}} \overline{u}^n_{\mu,i,K} = 1 \quad \forall K \in \mathcal{T}_h, \quad \forall n \in [\![0, N_t]\!], \tag{3.8}$$

which is the analogous version of (P2^h) for the SP-ROM.

Let us now explain in details how the vector $\boldsymbol{c}^n_\mu$ is computed. For any $\boldsymbol{c} := (c^k)_{1\le k\le r_\star} \in \mathbb{R}^{r_\star}$, let us introduce $\overline{\boldsymbol{Z}}(\boldsymbol{c}) := \left(\overline{z}_{i,K}(\boldsymbol{c})\right)_{K\in\mathcal{T}_h,\ 1\le i\le N_{\rm s}} \in \mathbb{R}^{N_h\times N_{\rm s}}$ the vector defined by

$$\overline{\boldsymbol{Z}}(\boldsymbol{c}) := \sum_{k=1}^{r_\star} c^k \boldsymbol{W}^k.$$

Moreover, we define $\overline{\boldsymbol{U}}(\boldsymbol{c}) := \left(\overline{u}_{i,K}(\boldsymbol{c})\right)_{K\in\mathcal{T}_h,\ 1\le i\le N_{\rm s}} \in \mathbb{R}^{N_h\times N_{\rm s}}$ by

$$\overline{u}_{i,K}(\boldsymbol{c}) := \frac{e^{\overline{z}_{i,K}(\boldsymbol{c})}}{\sum_{j=1}^{N_{\rm s}} e^{\overline{z}_{j,K}(\boldsymbol{c})}}, \quad \forall K \in \mathcal{T}_h,\ \forall i \in [\![1, N_{\rm s}]\!]. \tag{3.9}$$

Let us now define for all $\mu \in \mathcal{P}$, $1 \le n \le N_t$, $1 \le i \le N_{\rm s}$ and $K \in \mathcal{T}_h$, the application $\overline{G}^n_{\mu,i,K} : \mathbb{R}^{r_\star} \to \mathbb{R}$ defined by

$$\overline{G}^n_{\mu,i,K}(\boldsymbol{c}) := m_K \frac{\overline{u}_{i,K}(\boldsymbol{c}) - \overline{u}^{n-1}_{\mu,i,K}}{\Delta t_n} + \sum_{\sigma\in\mathcal{E}^K_h} F_{\mu,i,K\sigma}\left(\overline{\boldsymbol{U}}(\boldsymbol{c})\right), \tag{3.10}$$

where $\overline{u}^0_{\mu,i,K}(\boldsymbol{c}) := u^0_{i,K}$, and by $\overline{G}^n_\mu(\boldsymbol{c}) := \left(\overline{G}^n_{\mu,i,K}(\boldsymbol{c})\right)_{K\in\mathcal{T}_h, 1\le i\le N_{\rm s}}$. Let us finally denote by $\overline{H}^n_\mu : \mathbb{R}^{r_\star} \to \mathbb{R}^{r_\star}$ the application such that, for all $\boldsymbol{c} \in \mathbb{R}^{r_\star}$, $\overline{H}^n_\mu = \left(\overline{H}^{n,l}_\mu(\boldsymbol{c})\right)_{1\le l\le r_\star}$ where for all $1 \le l \le r_\star$,

$$\overline{H}^{n,l}_\mu(\boldsymbol{c}) := \left\langle \boldsymbol{W}^l, \overline{G}^n_\mu(\boldsymbol{c})\right\rangle,$$

where $\langle\cdot,\cdot\rangle$ denotes the euclidean scalar product of $\mathbb{R}^{N_h\times N_{\rm s}}$. Then, the vector $\boldsymbol{c}^n_\mu \in \mathbb{R}^{r_\star}$ is defined as a solution to

$$\overline{H}^n_\mu(\boldsymbol{c}^n_\mu) = 0, \tag{3.11}$$

and the numerical approximation $\overline{\boldsymbol{U}}^n_\mu$ of $\boldsymbol{U}^n_\mu$ given by the SP-ROM is given by (3.6) with $\overline{\boldsymbol{Z}}^n_\mu$ defined by (3.5). A solution to problem (3.11) is computed using a classical Newton algorithm.

The following proposition states that the SP-ROM indeed produces an approximation $\overline{\boldsymbol{U}}^n_\mu$ of $\boldsymbol{U}^n_\mu$ which enables to preserve analogous properties to (P1^h)-(P2^h)-(P3^h) on the level of the reduced-order model.

Proposition 3.1. *Let $\mu \in \mathcal{P}$ and let $\left(\overline{\boldsymbol{U}}_\mu^n\right)_{1\le n\le N_t}$ be the solution of the SP-ROM described above. Then, denoting by $\overline{\boldsymbol{U}}_\mu^n := \left(\overline{u}_{\mu,i,K}^n\right)_{K\in\mathcal{T}_h, 1\le i\le N_s}$ for all $1 \le n \le N_t$, the following properties hold:*

(P1$^{\mathrm{red}}$) ***mass conservation:***

$$\sum_{K\in\mathcal{T}_h} m_K \overline{u}_{\mu,i,K}^n = \sum_{K\in\mathcal{T}_h} m_K u_{\mu,i,K}^0 = \int_\Omega u_i^0(x)\,\mathrm{d}x \quad \forall i \in [\![1, N_s]\!], \quad \forall n \in [\![0, N_t]\!]. \tag{3.12}$$

(P2$^{\mathrm{red}}$) ***volume-filling constraint:***

$$\overline{u}_{\mu,i,K}^n > 0 \quad \forall K \in \mathcal{T}_h, \quad \forall i \in [\![1, N_s]\!], \quad \forall n \in [\![0, N_t]\!], \tag{3.13}$$

and

$$\sum_{i=1}^{N_s} \overline{u}_{\mu,i,K}^n = 1 \quad \forall K \in \mathcal{T}_h, \quad \forall n \in [\![0, N_t]\!]. \tag{3.14}$$

(P3$^{\mathrm{red}}$) ***entropy-entropy dissipation inequality:*** *For all $1 \le n \le N_t$, it holds that*

$$\frac{1}{\Delta t_n}(E_{\mathcal{T}_h}(\overline{\boldsymbol{U}}_\mu^n) - E_{\mathcal{T}_h}(\overline{\boldsymbol{U}}_\mu^{n-1})) + a_\mu^\star \sum_{\sigma\in\mathcal{E}_h} \sum_{i=1}^{N_s} \overline{u}_{\mu,i,\sigma}^n |D_{K\sigma} \ln(\overline{\boldsymbol{u}}_{\mu,i}^n)|^2 \le 0, \quad \forall n \in [\![1, N_t]\!]. \tag{3.15}$$

The next section is devoted to the proof of Proposition 3.1.

3.3 Proof of Proposition 3.1

Before proving Proposition 3.1 we introduce the following intermediate results.

Lemma 3.2. *Let $\boldsymbol{e} = (e_K)_{K\in\mathcal{T}_h}, \boldsymbol{v} = (v_K)_{K\in\mathcal{T}_h} \in \mathbb{R}^{N_h}$. Then,*

$$\sum_{K\in\mathcal{T}_h} \sum_{\sigma\in\mathcal{E}_h^K\cap\mathcal{E}_h^{\mathrm{int}}} e_K D_{K\sigma}\boldsymbol{v} = -\sum_{\sigma\in\mathcal{E}_h^{\mathrm{int}},\, \sigma=K|L} D_{K\sigma}\boldsymbol{e} D_{K\sigma}\boldsymbol{v}. \tag{3.16}$$

Proof. We have

$$\sum_{K\in\mathcal{T}_h} \sum_{\sigma\in\mathcal{E}_h^K\cap\mathcal{E}_h^{\mathrm{int}}} e_K D_{K\sigma}\boldsymbol{v} = \sum_{K\in\mathcal{T}_h} \sum_{\sigma\in\mathcal{E}_h^K\cap\mathcal{E}_h^{\mathrm{int}}} e_K\left(v_{K\sigma} - v_K\right).$$

Next, observe that for $\sigma \in \mathcal{E}_h^{\mathrm{int}}$ such that $\sigma = K|L$, we have,

$$e_K(v_{K\sigma} - v_K) + e_L(v_{L\sigma} - v_L) = -\left(e_K - e_L\right)\left(v_K - v_L\right) = -D_{K\sigma}\boldsymbol{e} D_{K\sigma}\boldsymbol{v}.$$

We sum on all internal edges to get the desired result. □

Lemma 3.3. *For all $\boldsymbol{U} := (u_{i,K})_{K\in\mathcal{T}_h, 1\le i\le N_s} \in \mathbb{R}^{N_h\times N_s}$ such that $\sum_{i=1}^{N_s} u_{i,K} = 1$ for all $K \in \mathcal{T}_h$, it holds that for all $K \in \mathcal{T}_h$ and all $\sigma \in \mathcal{E}_h^K \cap \mathcal{E}_h^{\mathrm{int}}$, we have*

$$\sum_{i=1}^{N_s} F_{\mu,i,K\sigma}(\boldsymbol{U}) = 0. \tag{3.17}$$

Proof. Let $\boldsymbol{U} := (u_{i,K})_{K\in\mathcal{T}_h, 1\le i\le N_s} \in \mathbb{R}^{N_h\times N_s}$ such that $\sum_{i=1}^{N_s} u_{i,K} = 1$ for all $K \in \mathcal{T}_h$. Then, it holds that

$$\begin{aligned}
\sum_{i=1}^{N_s} F_{\mu,i,K\sigma}(\boldsymbol{U}) &= \sum_{i=1}^{N_s} -a_\mu^\star \tau_\sigma D_{K\sigma}\boldsymbol{u}_i - \tau_\sigma \sum_{i=1}^{N_s}\left(\sum_{j=1, j\neq i}^{N_s} \left(a_{ij} - a_\mu^\star\right)\left(u_{j,\sigma} D_{K\sigma}\boldsymbol{u}_i - u_{i,\sigma} D_{K\sigma}\boldsymbol{u}_j\right)\right) \\
&= -a_\mu^\star \tau_\sigma D_{K\sigma}\left(\sum_{i=1}^{N_s} \boldsymbol{u}_i\right) - \tau_\sigma\left(\sum_{i=1}^{N_s}\sum_{j=1, j\neq i}^{N_s} \left(a_{ij} - a_\mu^\star\right)\left(u_{j,\sigma} D_{K\sigma}\boldsymbol{u}_i - u_{i,\sigma} D_{K\sigma}\boldsymbol{u}_j\right)\right).
\end{aligned}$$

We first have $D_{K\sigma}\left(\sum_{i=1}^{N_s} \boldsymbol{u}_i\right) = 0$ since $\sum_{i=1}^{N_s} u_{i,K} = 1$ for all $K \in \mathcal{T}_h$. Furthermore,

$$\sum_{i=1}^{N_s} \sum_{j=1, j\neq i}^{N_s} \left(a_{ij} - a_\mu^\star\right)\left(u_{j,\sigma} D_{K\sigma}\boldsymbol{u}_i - u_{i,\sigma} D_{K\sigma}\boldsymbol{u}_j\right) = 0,$$

since $a_{ij} = a_{ji}$ for all $1 \leq i, j \leq N_s$. Hence the result. □

We are now in position to prove Proposition 3.1.

Proof of Proposition 3.1. First, we observe that (P2$^{\rm red}$) can be easily checked using (3.9). We are thus left to prove (P1$^{\rm red}$) and (P3$^{\rm red}$). On the one hand, we have for all $1 \leq i \leq N_s$, since $\overline{\boldsymbol{U}}_\mu^n = \overline{\boldsymbol{U}}(\boldsymbol{c}_\mu^n)$,

$$\left\langle \boldsymbol{W}^{r+i}, \overline{G}_\mu^n(\overline{\boldsymbol{U}}_\mu^n)\right\rangle = \sum_{K\in\mathcal{T}_h} m_K \frac{\overline{u}_{\mu,i,K}^n - \overline{u}_{\mu,i,K}^{n-1}}{\Delta t_n} + \sum_{K\in\mathcal{T}_h} \sum_{\sigma\in\mathcal{E}_h^K\cap\mathcal{E}_h^{\rm int}} F_{\mu,i,K\sigma}(\overline{\boldsymbol{U}}_\mu^n) = 0 \quad \forall 1 \leq i \leq N_s.$$

Let us prove here that

$$\sum_{K\in\mathcal{T}_h} \sum_{\sigma\in\mathcal{E}_h^K\cap\mathcal{E}_h^{\rm int}} F_{\mu,i,K\sigma}(\overline{\boldsymbol{U}}_\mu^n) = 0. \tag{3.18}$$

Indeed, it holds that

$$\sum_{K\in\mathcal{T}_h} \sum_{\sigma\in\mathcal{E}_h^K\cap\mathcal{E}_h^{\rm int}} F_{\mu,i,K\sigma}(\overline{\boldsymbol{U}}_\mu^n) = \sum_{\sigma\in\mathcal{E}_h^{\rm int},\ \sigma=K|L} \left(F_{\mu,i,K\sigma}(\overline{\boldsymbol{U}}_\mu^n) + F_{\mu,i,L\sigma}(\overline{\boldsymbol{U}}_\mu^n)\right).$$

Furthermore, for all $\sigma = K|L \in \mathcal{E}_h^{\rm int}$, it holds that $F_{\mu,i,K\sigma}(\overline{\boldsymbol{U}}_\mu^n) + F_{\mu,i,L\sigma}(\overline{\boldsymbol{U}}_\mu^n) = 0$ from Remark 2.4. As a consequence, we obtain that

$$\sum_{K\in\mathcal{T}_h} m_K \overline{u}_{\mu,i,K}^n = \sum_{K\in\mathcal{T}_h} m_K \overline{u}_{\mu,i,K}^{n-1}. \tag{3.19}$$

Reasoning by induction, we then obtain that

$$\sum_{K\in\mathcal{T}_h} m_K \overline{u}_{\mu,i,K}^n = \sum_{K\in\mathcal{T}_h} m_K \overline{u}_{\mu,i,K}^0 = \sum_{K\in\mathcal{T}_h} m_K u_{\mu,i,K}^0 = \int_\Omega u_i^0(x)\,{\rm d}x.$$

Hence (P1$^{\rm red}$).

Let us now prove (P3$^{\rm red}$). It holds that

$$E_{\mathcal{T}_h}(\overline{\boldsymbol{U}}_\mu^n) - E_{\mathcal{T}_h}(\overline{\boldsymbol{U}}_\mu^{n-1}) = \sum_{K\in\mathcal{T}_h} \sum_{i=1}^{N_s} m_K \left(\overline{u}_{\mu,i,K}^n \ln(\overline{u}_{\mu,i,K}^n) - \overline{u}_{\mu,i,K}^{n-1} \ln(\overline{u}_{\mu,i,K}^{n-1})\right). \tag{3.20}$$

Besides, the coefficients $\overline{\boldsymbol{c}}_\mu^n$ are solution to $\overline{H}_\mu^n(\overline{\boldsymbol{c}}_\mu^n) = 0$. As a consequence, $\left(\sum_{l=1}^{r_\star} \overline{c}_\mu^{l,n} \boldsymbol{W}^l\right)^T \overline{G}_\mu^n(\overline{\boldsymbol{U}}_\mu^n) = 0$, which equivalently reads as

$$\sum_{i=1}^{N_s} \sum_{K\in\mathcal{T}_h} \overline{z}_{\mu,i,K}^n G_{i,K}^n(\overline{\boldsymbol{U}}_\mu^n) = 0.$$

Using (2.17) and introducing the notation $\overline{\rho}_{\mu,K}^n := \sum_{j=1}^{N_s} \exp(\overline{z}_{\mu,j,K}^n)$, we get $A + B = 0$ with

$$A := \sum_{i=1}^{N_s} \sum_{K\in\mathcal{T}_h} \ln(\overline{u}_{\mu,i,K}^n) \left(m_K \frac{\overline{u}_{\mu,i,K}^n - \overline{u}_{\mu,i,K}^{n-1}}{\Delta t_n} + \sum_{\sigma\in\mathcal{E}_h^K\cap\mathcal{E}_h^{\rm int}} F_{\mu,i,K\sigma}(\overline{\boldsymbol{U}}_\mu^n)\right) \tag{3.21}$$

and

$$B := \sum_{i=1}^{N_s} \sum_{K\in\mathcal{T}_h} \ln(\overline{\rho}^n_{\mu,K}) \left(m_K \frac{\overline{u}^n_{\mu,i,K} - \overline{u}^{n-1}_{\mu,i,K}}{\Delta t_n} + \sum_{\sigma\in\mathcal{E}_h^K\cap\mathcal{E}_h^{\rm int}} F_{\mu,i,K\sigma}(\overline{\boldsymbol{U}}^n_\mu) \right).$$

Employing (3.19) and Lemma (3.3), we have $B = 0$ so that $A = 0$. Therefore, it holds that

$$\sum_{i=1}^{N_s} \sum_{K\in\mathcal{T}_h} \ln(\overline{u}^n_{\mu,i,K}) \left(m_K \frac{\overline{u}^n_{\mu,i,K} - \overline{u}^{n-1}_{\mu,i,K}}{\Delta t_n} \right) + \sum_{i=1}^{N_s} \sum_{K\in\mathcal{T}_h} \ln(\overline{u}^n_{\mu,i,K}) \sum_{\sigma\in\mathcal{E}_h^K\cap\mathcal{E}_h^{\rm int}} F_{\mu,i,K\sigma}(\overline{\boldsymbol{U}}^n_\mu) = 0.$$

Furthermore, we have

$$F_{\mu,i,K\sigma}(\overline{\boldsymbol{U}}^n_\mu) := -a^\star_\mu \tau_\sigma \overline{u}^n_{i,\sigma} D_{K\sigma}\left(\ln(\overline{\boldsymbol{u}}^n_{\mu,i})\right) - \tau_\sigma \left(\sum_{j=1,\, j\neq i}^{N_s} \left(a_{ij} - a^\star_\mu\right) \overline{u}^n_{\mu,j,\sigma} \overline{u}^n_{\mu,i,\sigma} \left(D_{K\sigma}\left(\ln(\overline{\boldsymbol{u}}^n_{\mu,i})\right) - D_{K\sigma}\left(\ln(\overline{\boldsymbol{u}}^n_{\mu,j})\right)\right)\right).$$

Thus,

$$A = \sum_{i=1}^{N_s} \sum_{K\in\mathcal{T}_h} \ln(\overline{u}^n_{\mu,i,K}) \left(m_K \frac{\overline{u}^n_{\mu,i,K} - \overline{u}^{n-1}_{\mu,i,K}}{\Delta t_n} \right) + A_1 + A_2 \tag{3.22}$$

with

$$A_1 := \sum_{i=1}^{N_s} \sum_{K\in\mathcal{T}_h} \ln(\overline{u}^n_{\mu,i,K}) \sum_{\sigma\in\mathcal{E}_h^K\cap\mathcal{E}_h^{\rm int}} \left(-a^\star_\mu \tau_\sigma \overline{u}^n_{\mu,i,\sigma} D_{K\sigma}\left(\ln(\overline{\boldsymbol{u}}^n_{\mu,i})\right)\right)$$

and

$$A_2 := \sum_{i=1}^{N_s} \sum_{K\in\mathcal{T}_h} \ln(\overline{u}^n_{\mu,i,K}) \sum_{\sigma\in\mathcal{E}_h^K\cap\mathcal{E}_h^{\rm int}} \tau_\sigma \left(\sum_{j=1, j\neq i}^{N_s} \left(a_{ij} - a^\star_\mu\right) \overline{u}^n_{\mu,j,\sigma} \overline{u}^n_{\mu,i,\sigma} \left(D_{K\sigma}\left(\ln(\overline{\boldsymbol{u}}^n_{\mu,i})\right) - D_{K\sigma}\left(\ln(\overline{\boldsymbol{u}}^n_{\mu,j})\right)\right)\right).$$

Besides,

$$A_2 = \sum_{i=1}^{N_s} \sum_{K\in\mathcal{T}_h} \sum_{\sigma\in\mathcal{E}_h^K\cap\mathcal{E}_h^{\rm int}} \tau_\sigma \left(\sum_{j=1,\, j\neq i}^{N_s} \left(a_{ij} - a^\star_\mu\right) \overline{u}^n_{\mu,j,\sigma} \overline{u}^n_{\mu,i,\sigma} \ln(\overline{u}^n_{\mu,i,K}) \left(D_{K\sigma}\left(\ln(\overline{\boldsymbol{u}}^n_{\mu,i}) - \ln(\overline{\boldsymbol{u}}^n_{\mu,j})\right)\right)\right). \tag{3.23}$$

Using Lemma 3.2, we get

$$A_2 = -\sum_{i=1}^{N_s} \sum_{\sigma\in\mathcal{E}_h^{\rm int}} \tau_\sigma \left(\sum_{j=1,\, j\neq i}^{N_s} \left(a_{ij} - a^\star_\mu\right) \overline{u}^n_{\mu,j,\sigma} \overline{u}^n_{\mu,i,\sigma} D_{K\sigma}(\ln(\overline{\boldsymbol{u}}^n_{\mu,i})) D_{K\sigma}\left(\ln(\overline{\boldsymbol{u}}^n_{\mu,i}) - \ln(\overline{\boldsymbol{u}}^n_{\mu,j})\right)\right),$$

and

$$A_1 = \sum_{i=1}^{N_s} \sum_{\sigma\in\mathcal{E}_h^{\rm int}} a^\star_\mu \tau_\sigma \overline{u}^n_{\mu,i,\sigma} D_{K\sigma}(\ln(\overline{\boldsymbol{u}}^n_{\mu,i})) D_{K\sigma}(\ln(\overline{\boldsymbol{u}}^n_{\mu,i})) = \sum_{i=1}^{N_s} \sum_{\sigma\in\mathcal{E}_h^{\rm int}} a^\star_\mu \tau_\sigma \overline{u}^n_{\mu,i,\sigma} \left(D_{K\sigma} \ln(\overline{\boldsymbol{u}}^n_{\mu,i})\right)^2.$$

Next, we develop the term $D_{K\sigma}\left(\ln(\overline{\boldsymbol{u}}_{\mu,i}^n)\right) D_{K\sigma}\left(\ln(\overline{\boldsymbol{u}}_{\mu,i}^n) - \ln(\overline{\boldsymbol{u}}_{\mu,j}^n)\right)$ to get

$$
\begin{aligned}
A_2 = &- \sum_{\sigma\in\mathcal{E}_h^{\rm int}} \sum_{1\le i\neq j\le N_{\rm s}} \tau_\sigma\left(a_{ij}-a_\mu^\star\right)\overline{u}_{\mu,j,\sigma}^n \overline{u}_{\mu,i,\sigma}^n \left(D_{K\sigma}(\ln(\overline{\boldsymbol{u}}_{\mu,i}^n)\right)^2 \\
&+ \sum_{\sigma\in\mathcal{E}_h^{\rm int}} \sum_{1\le i\neq j\le N_{\rm s}} \tau_\sigma\left(a_{ij}-a_\mu^\star\right)\overline{u}_{\mu,j,\sigma}^n \overline{u}_{\mu,i,\sigma}^n D_{K\sigma}(\ln(\overline{\boldsymbol{u}}_{\mu,i}^n)) D_{K\sigma}\left(\ln(\overline{\boldsymbol{u}}_{\mu,j}^n)\right) \\
= &- \sum_{\sigma\in\mathcal{E}_h^{\rm int}} \frac{1}{2} \sum_{1\le i\neq j\le N_{\rm s}} \tau_\sigma\left(a_{ij}-a_\mu^\star\right)\overline{u}_{\mu,j,\sigma}^n \overline{u}_{\mu,i,\sigma}^n \left(D_{K\sigma}(\ln(\overline{\boldsymbol{u}}_{\mu,i}^n)\right)^2 \\
&+ \sum_{\sigma\in\mathcal{E}_h^{\rm int}} \frac{1}{2}\times 2 \sum_{1\le i\neq j\le N_{\rm s}} \tau_\sigma\left(a_{ij}-a_\mu^\star\right)\overline{u}_{\mu,j,\sigma}^n \overline{u}_{\mu,i,\sigma}^n D_{K\sigma}(\ln(\overline{\boldsymbol{u}}_{\mu,i}^n)) D_{K\sigma}\left(\ln(\overline{\boldsymbol{u}}_{\mu,j}^n)\right) \\
&- \sum_{\sigma\in\mathcal{E}_h^{\rm int}} \frac{1}{2} \sum_{1\le i\neq j\le N_{\rm s}} \tau_\sigma\left(a_{j,i}-a_\mu^\star\right)\overline{u}_{\mu,j,\sigma}^n \overline{u}_{\mu,i,\sigma}^n \left(D_{K\sigma}\ln(\overline{\boldsymbol{u}}_{\mu,j}^n)\right)^2.
\end{aligned}
$$

We thus obtain

$$
A_2 = - \sum_{\sigma\in\mathcal{E}_h^{\rm int}} \frac{1}{2} \sum_{1\le i\neq j\le N_{\rm s}} \tau_\sigma\left(a_{ij}-a_\mu^\star\right)\overline{u}_{\mu,j,\sigma}^n \overline{u}_{\mu,i,\sigma}^n \left(D_{K\sigma}(\ln(\overline{\boldsymbol{u}}_{\mu,i}^n)) - D_{K\sigma}(\ln(\overline{\boldsymbol{u}}_{\mu,j}^n))\right)^2.
$$

Now, let us consider again the equality (3.20). It follows from the convexity of the function $h : \mathbb{R}_+^* \ni x \mapsto x\ln(x)$ that

$$
\overline{u}_{\mu,i,K}^n - \overline{u}_{\mu,i,K}^{n-1} + \overline{u}_{\mu,i,K}^n \ln(\overline{u}_{\mu,i,K}^n) - \overline{u}_{\mu,i,K}^{n-1}\ln(\overline{u}_{\mu,i,K}^n) \ge \overline{u}_{\mu,i,K}^n \ln(\overline{u}_{\mu,i,K}^n) - \overline{u}_{\mu,i,K}^{n-1}\ln(\overline{u}_{\mu,i,K}^{n-1}). \tag{3.24}
$$

Thus, employing (3.24) and the mass conservation property (3.19), we obtain that

$$
E_{\mathcal{T}_h}(\overline{\boldsymbol{U}}_\mu^n) - E_{\mathcal{T}_h}(\overline{\boldsymbol{U}}_\mu^{n-1}) \le \Delta t_n \sum_{K\in\mathcal{T}_h}\sum_{i=1}^{N_{\rm s}} m_K \ln(\overline{u}_{\mu,i,K}^n)\left(\frac{\overline{u}_{\mu,i,K}^n - \overline{u}_{\mu,i,K}^{n-1}}{\Delta t}\right) = \Delta t(A_2 - A_1).
$$

Using (3.22) yields

$$
E_{\mathcal{T}_h}(\overline{\boldsymbol{U}}_\mu^n) - E_{\mathcal{T}_h}(\overline{\boldsymbol{U}}_\mu^{n-1}) + \Delta t_n a_\mu^\star \sum_{\sigma\in\mathcal{E}_h^{\rm int}}\sum_{i=1}^{N_{\rm s}} \tau_\sigma \overline{u}_{\mu,i,\sigma}^n \left(D_{K\sigma}\ln(\overline{\boldsymbol{u}}_{\mu,i}^n)\right)^2 \le \Delta t_n A_2 \le 0.
$$

Hence (P3$^{\rm red}$) and the desired result. □

4 Numerical experiments

This section numerically illustrates our theoretical developments. All the tests have been performed using the Python code and can be found at url `https://jdabaghi.github.io/`. We consider two different test cases with respectively $N_{\rm s} = 3$ and $N_{\rm s} = 4$ that are reported respectively in Section 4.1 and Section 4.2.

We consider a one-dimensional domain $\Omega = (0,1)$. We consider a uniform spatial discretization grid of step $\Delta x = 10^{-2}$ so that the total number of cells is equal to 10^2. We use the Newton solver described in Section 2.2.3 combined with the GMRES linear solver [30, 28, 19]. The main reason of such a choice is to speed up the resolution of the linear system stemming from the Newton method. Our Newton solver thus enters in the wide category of inexact Newton solvers [7, 8, 9, 20]. We make use of the following criterion: $\sup|\boldsymbol{U}_\mu^{n,k} - \boldsymbol{U}_\mu^{n,k-1}| < \varepsilon_{\rm lin}$ with $\varepsilon_{\rm lin} = 10^{-8}$, where $\boldsymbol{U}_\mu^{n,k} \in \mathbb{R}^{N_h\times N_{\rm s}}$ is the approximate solution provided by the Newton solver at a given step $k \ge 1$. In both test cases, we compare the POD reduced-order model described in Section 3.1 and the SP reduced-order model we propose in Section 3.2. In particular, we numerically illustrate the fact that the SP reduced model of satisfies the structural properties of the discrete solution listed in Lemma 3.1.

The value of the parameter $a_\mu^\star > 0$ raised in (2.9) is chosen as follows

$$
a_\mu^\star := \min\left\{\max_{i\neq j} a_{ij}, \max\left\{\min_{i\neq j} a_{ij}, \frac{1}{2}\frac{\Delta x^2}{\Delta t_n}\right\}\right\}, \tag{4.1}
$$

as suggested in [6]. We refer to [6] for a complete discussion.

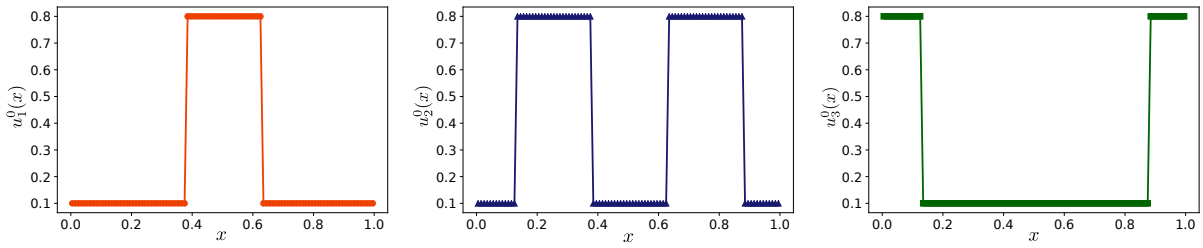

Figure 1: Initial condition for test case 1.

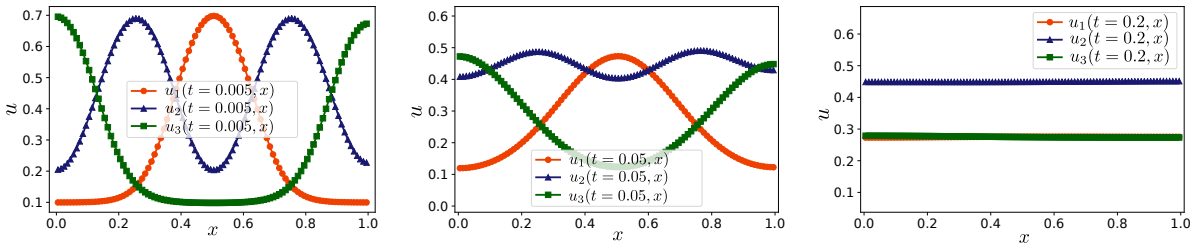

Figure 2: $u_1(t,x)$, $u_2(t,x)$, and $u_3(t,x)$ at different values of the time t. $t = 0.005$ (left), $t = 0.05$ (middle), and $t = 0.2$ (right).

4.1 Test case 1: three species

In this first test case, the initial guess is chosen as

$$u_1^0(x) := \begin{cases} 1-2\delta & \text{if } x \in \left[\frac{3}{8}, \frac{5}{8}\right] \\ \delta & \text{else,} \end{cases} \quad u_2^0(x) := \begin{cases} 1-2\delta & \text{if } x \in \left[\frac{1}{8}, \frac{3}{8}\right] \cap \left[\frac{5}{8}, \frac{7}{8}\right] \\ \delta & \text{else} \end{cases} \tag{4.2}$$

and

$$u_3^0(x) := \begin{cases} 1-2\delta & \text{if } x \in \left[0, \frac{1}{8}\right] \cap \left[\frac{7}{8}, 1\right] \\ \delta & \text{else.} \end{cases} \tag{4.3}$$

Note that the initial solution u^0 satisfies the volume filling constraint property [$(P2)$] of Section 2.1. The final simulation time is $T := 0.5$ and we use a constant time step $\Delta t = \Delta t_n := 5 \times 10^{-4}$ so that $N_t = 10^3$. Within the offline stage, we compute 20 snapshots of solutions, i.e. we compute the collection $\left(\boldsymbol{U}_\mu^n\right)_{1 \le n \le N_t}$ for all μ belonging to a subset $\mathcal{P}_{\text{train}} \subset \mathcal{P}$ so that $\text{Card}(\mathcal{P}_{\text{train}}) = 20$. For the sake of clarity, the elements of $\mathcal{P}_{\text{train}}$ which are in fact $N_s \times N_s$ matrices, are determined by selecting random numbers in the set $[0, 1]$. More precisely, as the matrices of $\mathcal{P}_{\text{train}}$ are symmetric with diagonal off coefficients $\frac{N_s \times (N_s - 1)}{2}$ real values belonging to the interval $[0, 1]$ are sampled. We denote in the following by $\mu^0, \cdots, \mu^{19}$ the elements of $\mathcal{P}_{\text{train}}$.

Note that for the definition of the initial guess, the parameter δ is chosen as $\delta = 0.1$. An illustration of the initial conditions u_1^0, u_2^0, and u_3^0 is provided in Figure 1.

4.1.1 The high-fidelity problem

In Figure 2, we represent the behavior of the numerical solution at several time steps for one selected parameter $\mu^0 \in \mathcal{P}_{\text{train}}$ and when the Newton solver and GMRES solver have converged. In fact, it corresponds to high-fidelity numerical solutions. In this case, the parameter $\mu^0 = (a_{ij}^0)_{1 \le i,j \le N_s}$ is given by

$$a_{12}^0 = 0.75, \quad a_{13}^0 = 0.73, \quad a_{23}^0 = 0.84. \tag{4.4}$$

We observe that the local volumic fractions evolve over time to reach constant profiles (around 0.44 for u_2, and around 0.26 for u_1 and u_3) in the long time limit. This behavior is typical of the solutions of the particular cross-diffusion system we consider here.

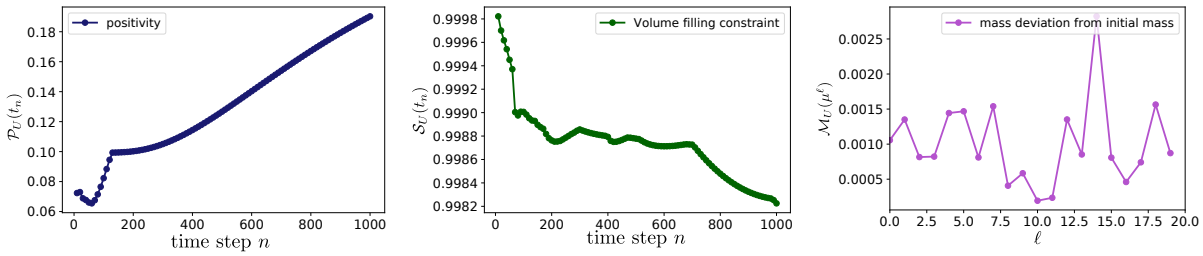

Figure 3: Properties of the fine numerical solution. Left : non-negativity of the solution, middle : preservation of the volume filling constraint, right : conservation of mass.

In Figure 3 we show that the numerical solution obtained by the finite volume resolution (see Section 2.2) preserves the structural properties listed in Section 2.2.2. We have simulated the cross-diffusion model (2.2) for all $\mu \in \mathcal{P}_{\text{train}}$. In the left figure, we have represented for each time step $n \in [\![1, N_t]\!]$, the following quantity:

$$\mathcal{P}_U(t_n) := \inf_{\mu\in\mathcal{P}_{\text{train}}} \inf_{1\le i\le N_s} \inf_{K\in\mathcal{T}_h} u^n_{\mu,i,K}. \tag{4.5}$$

We observe that the functional $\mathcal{P}_U$ reaches its minimum around $0.065 > 0$ so the numerical solution is always positive. In the middle figure is displayed the quantity

$$\mathcal{S}_U(t_n) := \inf_{\mu\in\mathcal{P}_{\text{train}}} \inf_{K\in\mathcal{T}_h} \sum_{i=1}^{N_s} u^n_{\mu,i,K} \tag{4.6}$$

for each time step $n \in [\![1, N_t]\!]$. In particular we observe that this quantity is very close to the optimal value of 1 which shows that the finite volume procedure described in Section 2.2 preserves the volume filling constraint. The right figure illustrates the mass conservation property. We have displayed for each parameter $\mu \in \mathcal{P}_{\text{train}}$ the maximal deviation of the mass from the initial mass. This maximal deviation is given by

$$\mathcal{M}_U(\mu) := \max_{i\in[\![1,N_s]\!]} \max_{n\in[\![1,N_t]\!]} \left| \sum_{K\in\mathcal{T}_h} m_K u^n_{\mu,i,K} - \int_\Omega u^0_i(x)\,\mathrm{dx} \right|. \tag{4.7}$$

We observe that this deviation of the mass is of order 10^{-4} or 10^{-3} which is very close to 0. It proves the consistency of the finite volume procedure described is Section 2.2.

Finally, Figure 4 is a complement to Figure 3 and shows the exponential decay of the entropy to a constant value. Recall that the entropy at time t_n is given by $E_{\mathcal{T}_h}(\boldsymbol{U}^n) := \sum_{K\in\mathcal{T}_h} \sum_{i=1}^{N_s} m_K u^n_{i,K} \ln(u^n_{i,K})$.

Note that the left-hand side figure corresponds to the cross-diffusion coefficients μ^0 defined by (4.4) whereas the middle and right figures corresponds to other sets of cross-diffusion coefficients: $\mu^9 = (a^9_{ij})_{1\le i\ne j\le N_s}$ and $\mu^{17} = (a^{17}_{ij})_{1\le i\ne j\le N_s}$, with

$$a^9_{12} = 0.93,\ a^9_{13} = 0.71,\ a^9_{23} = 0.44 \quad \text{and} \quad a^{17}_{12} = 0.37,\ a^{17}_{13} = 0.004,\ a^{17}_{23} = 0.72. \tag{4.8}$$

4.1.2 The POD reduced order model

In this section, we show that the first POD reduced-order model does not preserve the structural properties of the solution.

In Figure 5 is displayed the violation of the structural properties of the solution for the first POD reduced model (see Section 3.1). For the middle and right figure, the cardinality of the reduced basis is $r = 1$. More precisely, in the middle figure, we have represented the quantity $\mathcal{S}_{\widetilde{U}}(t_n)$ (see (4.6)) as a function of $n \in [\![1, N_t]\!]$. We observe that $\mathcal{S}_{\widetilde{U}}(t_n) \ne 1$ for many time steps so that the volume filling constraint is violated. On the right figure, we show the deviation of the mass $\mathcal{M}_{\widetilde{U}}(\mu)$ (see (4.7)) of the reduced problem from the initial mass $\sum_{K\in\mathcal{T}_h} m_K \widetilde{u}^0_{\mu,i,K}$. This deviation could be important for several values of μ so that

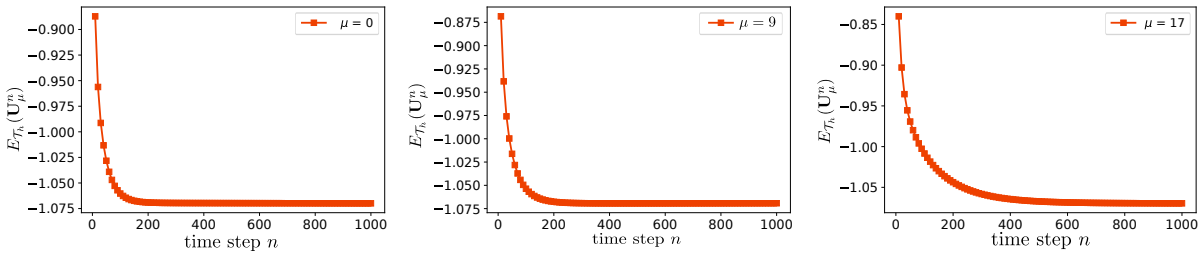

Figure 4: Entropy functional for three values of the parameters $\mu \in \mathcal{P}_{\text{train}}$.

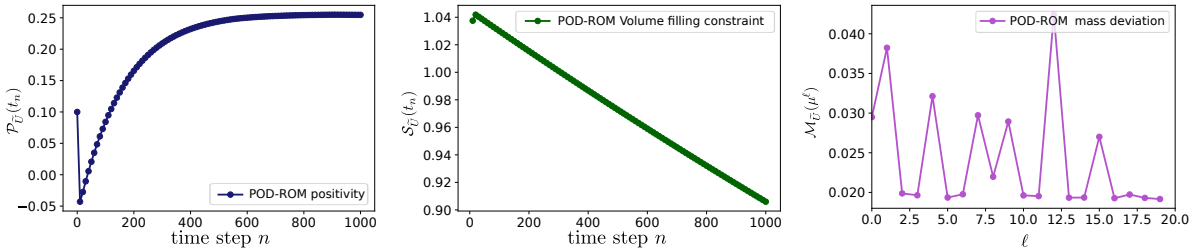

Figure 5: Violation of the physical properties of the reduced solution. Left : violation of the positivity, middle : violation of the volume filling constraint, right : violation of the conservation of mass.

the mass conservation property is violated. On the left figure, we considered a case where $r = 2$. The quantity $\mathcal{P}_{\widetilde{U}}(t_n)$ (see (4.5)) is plotted as a function of $n \in [\![1, N_t]\!]$. Here also, we observe that the positivity constraint is violated. Note that here we have considered two basis functions because for one basis function the positivity occurs everywhere. It is a surprising and unexpected result.

Finally, in Figure 6 we show (left figure and middle figure) when $r = 1$ that the discrete entropy functional defined by (2.15) (where $\boldsymbol{U}$ is replaced by $\widetilde{\boldsymbol{U}}_\mu^n$) is not a decreasing function. The right part of Figure 6 shows that the error between the reduced model and the fine resolution defined by

$$\max_{i\in[\![1,N_s]\!]} \left\| u_\mu^i - \tilde{u}_\mu^i \right\|_{L^\infty(\mathcal{P}_{\text{train}},L^2(\Omega),L^\infty([0,T]))} := \max_{i\in[\![1,N_s]\!]} \max_{\mu\in\mathcal{P}_{\text{train}}} \max_{n\in[\![1,N_t]\!]} \left(\sum_{K\in\mathcal{T}_h} \left| u_{\mu,i,K}^n - \widetilde{u}_{\mu,i,K}^n \right|^2 \right)^{\frac{1}{2}} \tag{4.9}$$

decreases when the dimension of the reduced basis increases. It begins to stall when $r = 20$. Here, u_μ^i respectively $\widetilde{u}_\mu^i$ is the functional representation of $\boldsymbol{U}_\mu^i := \left(u_{\mu,i,K}^n\right)_{\mu\in\mathcal{P}_{\text{train}},K\in\mathcal{T}_h,n\in[\![1,N_t]\!]}$ respectively $\widetilde{\boldsymbol{U}}_\mu^i := \left(\widetilde{u}_{\mu,i,K}^n\right)_{\mu\in\mathcal{P}_{\text{train}},K\in\mathcal{T}_h,n\in[\![1,N_t]\!]}$.

4.1.3 SP reduced-order model

In this section, we propose numerical experiments for the structure preserving reduced order model described in Section 3.2.

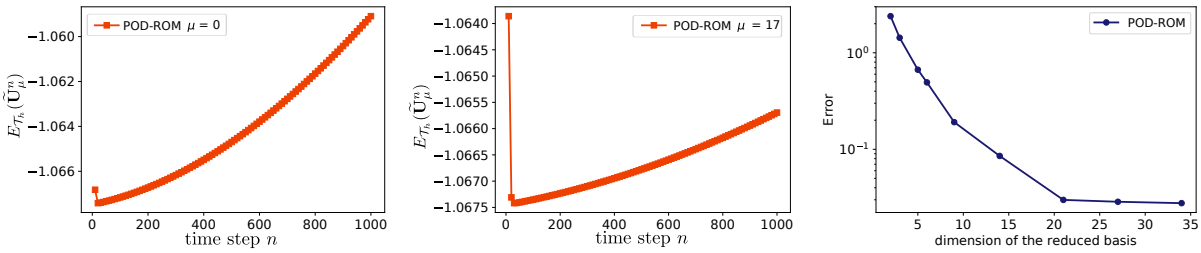

Figure 6: Violation of the decay of entropy and reduced model error.

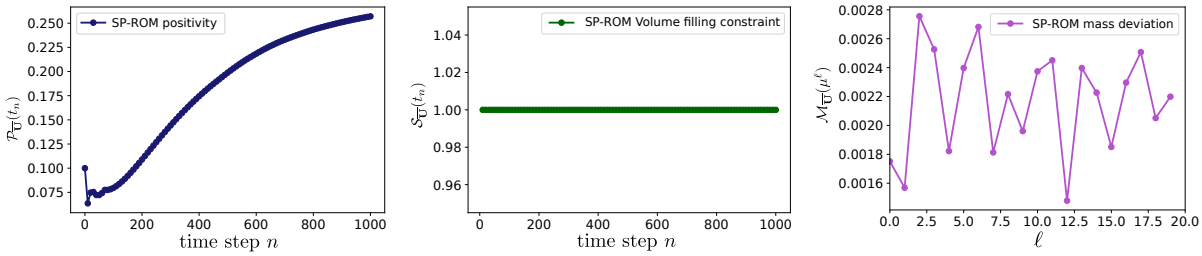

Figure 7: Preservation of the structural properties of the reduced solution. Left : positivity property, middle : volume filling constraint, right : conservation of mass.

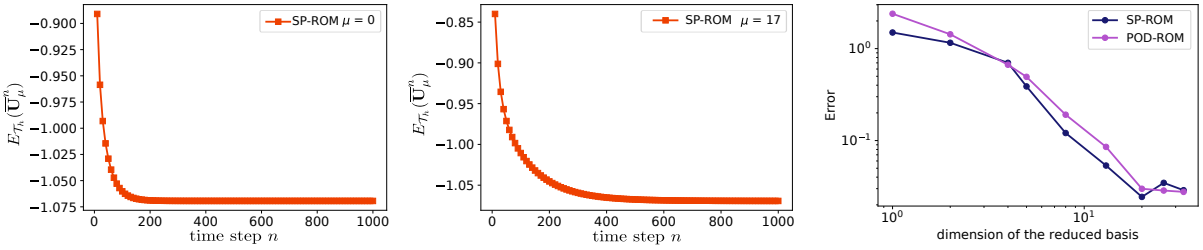

Figure 8: Preservation of the entropy property : left and middle. Error of the reduced model : right.

Figure 7 is the analog of Figure 5 where we observe that the first three structural properties listed in Lemma 3.1 are satisfied. In the left figure, $r = 1$, and in the middle and right figure $r = 2$. Here, we employ (4.5), (4.6) and (4.7) with $\overline{\boldsymbol{U}}_\mu^n$ instead of $\widetilde{\boldsymbol{U}}_\mu^n$.

Next, we represent in Figure 8 the evolution of the entropy functional for the cross-diffusion coefficients μ^0 defined by (4.4) and μ^{17} defined by (4.8) where the reduced solution is provided by the SP-reduced model of Section 3.2. In particular, we observe that the entropy decreases exponentially before reaching a constant profile, as for the high-fidelity model. The right figure compares the behavior of the two reduced-order model error. The blue curve corresponds to the error provided by the SP-ROM and the violet curve corresponds to the error provided by the POD-ROM (this time we use (4.9) but with $\overline{u}_\mu^i$ instead of $\widetilde{u}_\mu^i$).

We see that the behavior of the two curves are similar with a higher accuracy for the SP-reduced model.

4.2 Test case 2: four species

In this test case, we consider $N_{\rm s} = 4$ species, like in the model used for the simulation of the PVD fabrication process of thin film solar cells proposed in [1]. The final simulation time is $T = 0.5$ and we use a constant time step $\Delta t = \Delta t_n = 2.5 \times 10^{-4}$ so that $N_t = 2 \times 10^3$.

We again use the Newton solver described in Section 2.2.3 combined with the GMRES linear solver for speeding the linear system resolution. In this Section, we compute 20 snapshots of solutions so that $\mathrm{Card}(\mathcal{P}_{\rm train}) = 20$. The definition of the parameter $a_\mu^\star$ follows (4.1). Concerning the initial conditions we take

$$w_1^0(x) := e^{-25(x-0.5)^2}, \quad w_2^0(x) := x^2 + \varepsilon, \quad w_3^0(x) := 1 - e^{-25(x-0.5)^2}, \quad w_4^0(x) := |\sin(\pi x)| \tag{4.10}$$

where $\varepsilon = 10^{-6}$, and define

$$u_i^0(x) = \frac{w_i^0(x)}{\sum_{l=1}^{N_{\rm s}} w_l^0(x)} \tag{4.11}$$

for all $1 \le i \le 4$ and $x \in (0,1)$.

In Figure 9 we represent the shape of the high-fidelity numerical solution at three time steps at $n = 20$, $n = 200$, and $n = 1700$. Here, the cross-diffusion coefficients $\mu^{17} = (a_{ij}^{17})_{1 \le i \ne j \le 4}$ are given by

$$a_{12}^{17} = 0.64, \ a_{13}^{17} = 0.31, \ a_{14}^{17} = 0.53, \ a_{23}^{17} = 0.99, \ a_{24}^{17} = 0.84, \ a_{34}^{17} = 0.99. \tag{4.12}$$

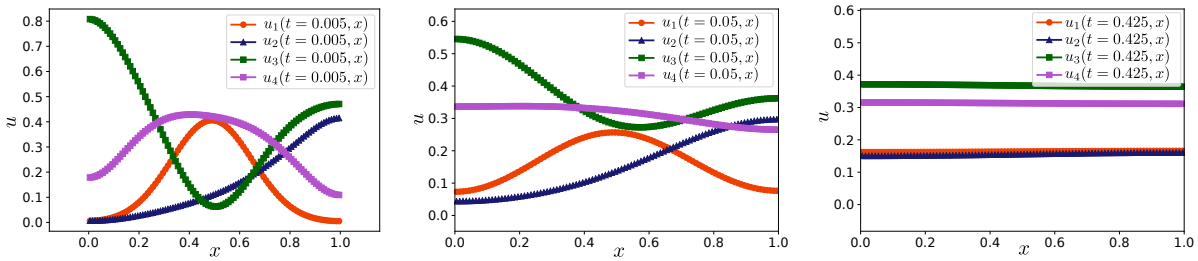

Figure 9: Profile of the numerical solution at $n = 20$ (left), $n = 200$ (middle), and $n = 1700$ (right) for the cross diffusion coefficients μ^{17}.

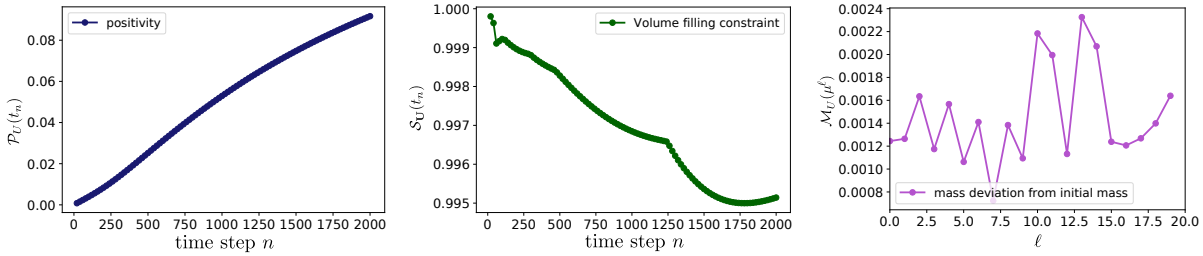

Figure 10: Properties of the fine numerical solution. Left: positivity of the solution, middle: preservation of the volume filling constraint, right: conservation of mass.

In Figure 10 are displayed the structural properties of the numerical solution, namely the positivity (left figure), the volume filling constraint (middle figure), and the mass conservation (right figure). As in Section 4.1.1, we observe that the three properties are preserved along the simulation.

In Figure 11 we represent the behavior of the entropy functional for three sets of cross-diffusion coefficients $\mu^0 := (a^0_{ij})_{1\le i\neq j\le 4}$, $\mu^8 := (a^8_{ij})_{1\le i\neq j\le 4}$, where

$$a^0_{12} = 0.36,\ a^0_{13} = 0.19,\ a^0_{14} = 0.64,\ a^0_{23} = 0.07,\ a^0_{24} = 0.61,\ a^0_{34} = 0.51,$$
$$a^8_{12} = 0.69,\ a^8_{13} = 0.30,\ a^8_{14} = 0.16,\ a^8_{23} = 0.37,\ a^8_{24} = 0.95,\ a^8_{34} = 0.38,$$

and μ^{17} defined in (4.12).

We observe again the fact that the entropy of the system converges exponentially fast to some limit value.

4.2.1 The POD reduced-order model

In Figure 12, we depict the violation of the structural properties of the numerical solution given by the POD-ROM. In the left Figure, we represent the number of cells where the solution could be negative as a

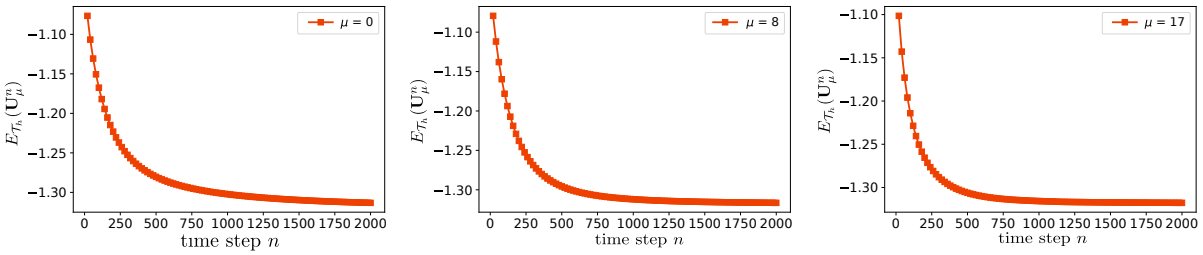

Figure 11: Entropy functional for three parameters.

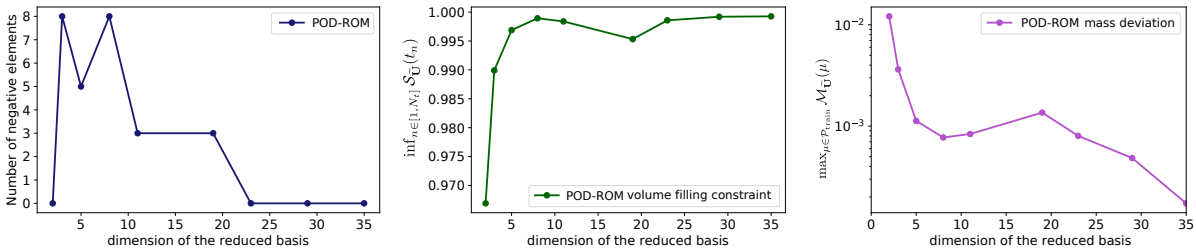

Figure 12: Violation of the physical properties of the POD-ROM. Left : violation of the positivity, middle : violation of the volume filling constraint, right : violation of the mass conservation.

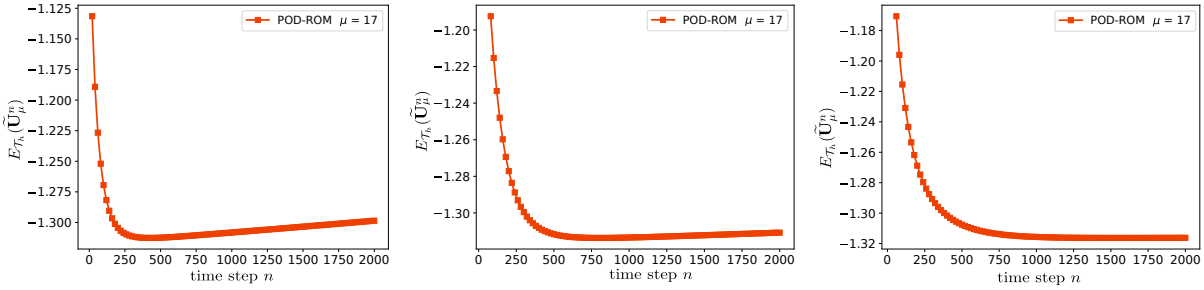

Figure 13: Violation of the decay of entropy for $r = 1$ (left), $r = 2$ (middle), $r = 4$ (right) and for POD-ROM.

function of the dimension of the reduced basis. More precisely, for each $r > 0$, is associated 20 set of N_t solutions. The results obtained in the left figure correspond to the number of negative values that appear in the whole set of $20 \times N_t$ possible vector of solutions.

We observe that for many configurations (from $r = 2$ to $r = 18$), we can find several negative elements. Also note that a surprising result occurs for the case $r = 1$. In this case, the solution remains always positive which is unexpected. The same phenomenon occured in the previous test case presented in Section 4.1.2. However, it is not recommended to consider only the reduced model formed by one element as it induces a numerical solution that does not preserve the volume filling constraint property as it is displayed in the middle figure, and the mass conservation expressed on the right figure. Note that in the middle figure is displayed the quantity $\inf_{n\in[\![1,N_t]\!]} \inf_{\mu\in\mathcal{P}_{\text{train}}} \inf_{K\in\mathcal{T}_h} \sum_{i=1}^{N_s} \widetilde{u}^n_{\mu,i,K}$ for several values of r. Concerning the mass deviation, we have represented the quantity $\max_{\mu\in\mathcal{P}_{\text{train}}} \mathcal{M}_{\widetilde{U}}(\mu)$ as a function of r where $\mathcal{M}_{\widetilde{U}}(\mu)$ is defined by (4.7). Thus, to obtain a reduced model respecting the first three properties of Lemma 3.1 we need to consider $r = 22$ basis vectors which is not appropriate. Figure 13 completes the results obtained from Figure 12. The discrete entropy functional is represented as a function of the time steps. We observe for $r = 1$ and $r = 2$ that the entropy increases beyond some time step which constitutes a physical violation.

4.2.2 The SP reduced-order model

This section is devoted to numerical experiments for the SP-reduced order model. We represent in Figure 14 the structural properties of the reduced solution. On the left Figure, we represented for several values of $r > 0$ the minimum value that can takes the numerical solution. More precisely we have represented the quantity

$$\inf_{n\in[\![1,N_t]\!]} \inf_{\mu\in\mathcal{P}_{\text{train}}} \inf_{K\in\mathcal{T}_h} \inf_{i\in[\![1,N_s]\!]} \overline{u}^n_{\mu,i,K}$$

for several values of $r > 0$. We observe that the solution is always nonnegative which shows that the positivity constraint is satisfied for this reduced model. In the middle Figure, is verified the volume filling constraint property. We displayed the quantity

$$\inf_{n\in[\![1,N_t]\!]} \inf_{\mu\in\mathcal{P}_{\text{train}}} \inf_{K\in\mathcal{T}_h} \sum_{i=1}^{N_s} \overline{u}^n_{\mu,i,K}$$

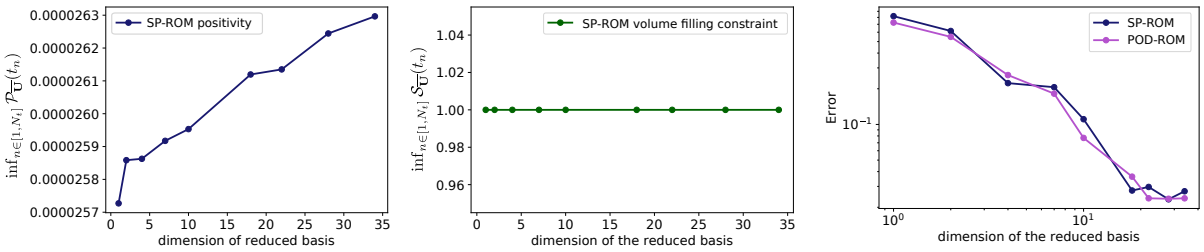

Figure 14: Preservation of the structural properties of the SP-ROM. Left : positivity property, middle : volume filling constraint, right : reduced model error.

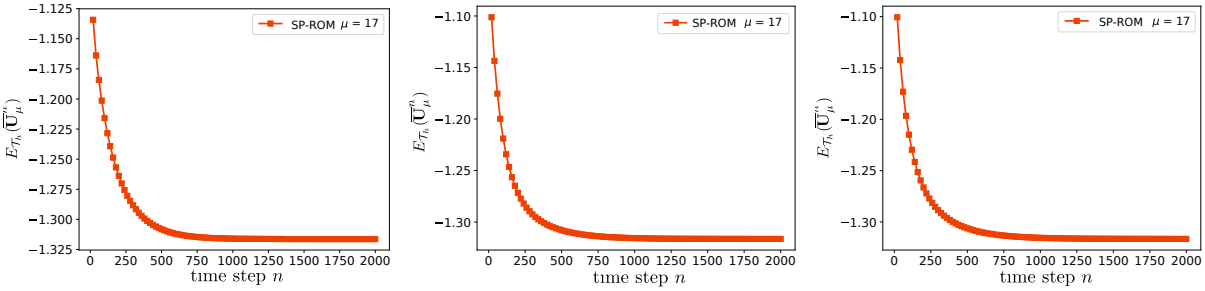

Figure 15: Entropy property of the SP-ROM. Left : $r = 1$, middle : $r = 2$, right : $r = 4$.

for several values of $r > 0$. We observe that this quantity is always equal to the optimal value of 1. Finally, in the right Figure we have represented the error of the two reduced models as a function of the cardinality of the reduced basis. Recall that these error are defined by (4.9). We observe that the error decreases when the dimension of the reduced basis r increases, at a similar rate for both approaches. Then, in Figure 15 we have illustrated the behavior of the discrete reduced entropy for the cross-diffusion coefficients μ^{17} defined by (4.12) and for $r = 1, 2, 4$. Contrary to Figure 13 we can see that the entropy is a decreasing function with respect to the time steps. Thus, our SP-ROM indeed preserves the structural properties of the numerical solution.

4.2.3 Validation stage

In this section, we check the validity of the various reduced-order models for cross-diffusion coefficients which do not belong to the training set $\mathcal{P}_{\text{train}}$. To this aim, we select values of parameters μ in a subset $\mathcal{P}_{\text{valid}}$ of $\mathcal{P}$, which is different from $\mathcal{P}_{\text{train}}$ and compare the error between the high-fidelity model and the ROMs. Here, $\text{Card}(\mathcal{P}_{\text{valid}}) = 20$ and to sample the coefficients of the cross-diffusion matrices we proceed as for the matrices of $\mathcal{P}_{\text{train}}$. The results reported in Figure 16 show that the solutions given by a fine resolution evolve to constant profiles which is the typical scenario of cross-diffusion system simulations.

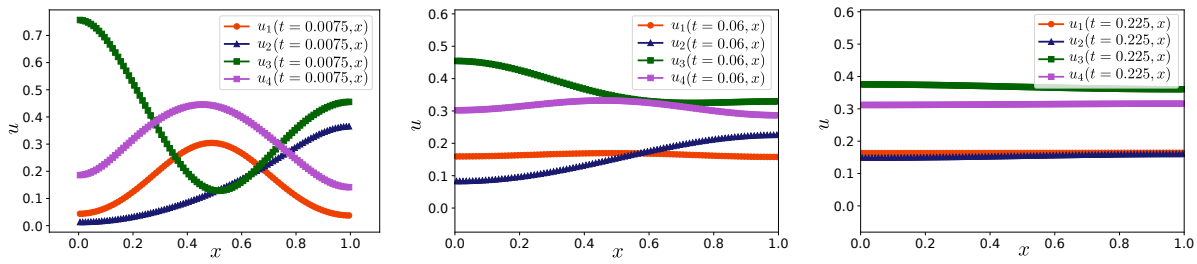

Figure 16: Profile of the numerical solution at $n = 30$ (left), $n = 240$ (middle), and $n = 900$ (right) for the cross-diffusion matrix $\mathbb{A}_{27}$.

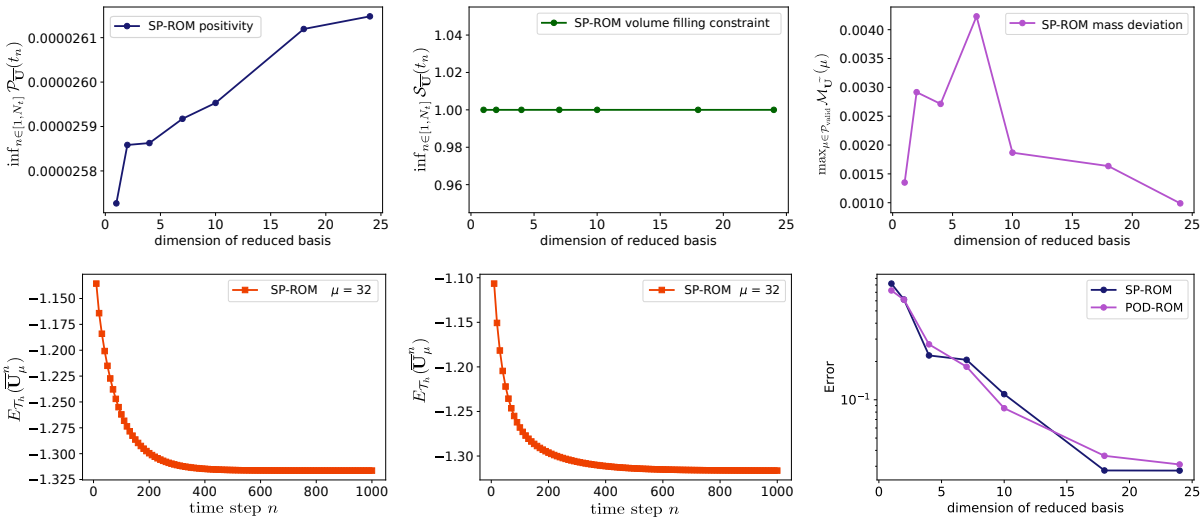

Figure 17: Validation stage for SP-ROM. Top left: positivity constraint, top middle : volume filling constraint property, top right : mass deviation, down left : entropy property for $r = 1$, down middle : entropy property for $r = 10$.

Figure 17 is the analog of Figure 15 and Figure 14. We observe that the positivity constraint, the volume filling constraint, and the mass conservation property are satisfied for each reduced model SP-ROM. Furthermore, the decay of entropy is also found back and we have displayed the particular case where the cross-diffusion coefficients $\mu^{32} = (a_{ij}^{32})_{1\leq i\neq j\leq 4}$ are defined by

$$a_{12}^{32} = 0.22,\ a_{13}^{32} = 0.37,\ a_{14}^{32} = 0.17,\ a_{23}^{32} = 0.53,\ a_{24}^{32} = 0.97,\ a_{34}^{32} = 0.82.$$

Finally, the results that we obtained for other parameters $\mu \in \mathcal{P}_{\text{valid}}$ are similar to the results obtained in the previous section with $\mu \in \mathcal{P}_{\text{train}}$. Also note that the error for the two reduced models have similar behavior.

5 Conclusion

In this work, we proposed a structure-preserving reduced-order model for a cross-diffusion system, which yields comparable accuracy with respect to a standard POD-ROM while preserving the main features of the original model. The numerical experiments confirmed the theoretical properties of the proposed approach. Several open questions remain to be tackled: first, for the SP-ROM to be online efficient, it will be needed to use it in conjunction with, for instance, the well-known Empirical Interpolation Method. It is not clear however how to design such a empirical interpolation method which would ensure that the resulting ROM would still preserve the desired properties such as non-negativeness of the solutions or entropy decay. Moreover, the design of appropriate a posteriori estimators would make possible the use of a greedy algorithm for the selection of the reduced basis, which would be cheaper that the POD selection which is done here. We leave these questions for future work.

References

[1] A. Bakhta and V. Ehrlacher, *Cross-diffusion systems with non-zero flux and moving boundary conditions*, ESAIM Math. Model. Numer. Anal., 52 (2018), pp. 1385–1415.

[2] J. W. Barrett and J. F. Blowey, *Finite element approximation of a nonlinear cross-diffusion population model*, Numerische Mathematik, 98 (2004), pp. 195–221.

[3] G. Berkooz, P. Holmes, and J. L. Lumley, *The proper orthogonal decomposition in the analysis of turbulent flows*, in Annual review of fluid mechanics, Vol. 25, Annual Reviews, Palo Alto, CA, 1993, pp. 539–575.

[4] M. Burger, M. Di Francesco, J.-F. Pietschmann, and B. Schlake, *Nonlinear cross-diffusion with size exclusion*, SIAM J. Math. Anal., 42 (2010), pp. 2842–2871.

[5] C. Cancès, V. Ehrlacher, and L. Monasse, *Finite volumes for the stefan-maxwell cross-diffusion system*, arXiv preprint arXiv:2007.09951, (2020).

[6] C. Cancès and B. Gaudeul, *A convergent entropy diminishing finite volume scheme for a cross-diffusion system*, SIAM J. Numer. Anal., 58 (2020), pp. 2684–2710.

[7] R. S. Dembo, S. C. Eisenstat, and T. Steihaug, *Inexact Newton methods*, SIAM J. Numer. Anal., 19 (1982), pp. 400–408.

[8] S. C. Eisenstat and H. F. Walker, *Globally convergent inexact Newton methods*, SIAM J. Optim., 4 (1994), pp. 393–422.

[9] ——, *Choosing the forcing terms in an inexact Newton method*, SIAM J. Sci. Comput., 17 (1996), pp. 16–32. Special issue on iterative methods in numerical linear algebra (Breckenridge, CO, 1994).

[10] R. Eymard, T. Gallouët, and R. Herbin, *Finite volume methods*, in Handbook of numerical analysis, Vol. VII, Handb. Numer. Anal., VII, North-Holland, Amsterdam, 2000, pp. 713–1020.

[11] L. Fick, Y. Maday, A. T. Patera, and T. Taddei, *A stabilized POD model for turbulent flows over a range of Reynolds numbers: optimal parameter sampling and constrained projection*, J. Comput. Phys., 371 (2018), pp. 214–243.

[12] R. L. FOX and H. MIURA, *An approximate analysis technique for design calculations*, AIAA Journal, 9 (1971), pp. 177–179.

[13] M. Gubisch and S. Volkwein, *Proper orthogonal decomposition for linear-quadratic optimal control*, in Model reduction and approximation, vol. 15 of Comput. Sci. Eng., SIAM, Philadelphia, PA, 2017, pp. 3–63.

[14] J. S. Hesthaven, G. Rozza, and B. Stamm, *Certified reduced basis methods for parametrized partial differential equations*, SpringerBriefs in Mathematics, Springer, Cham; BCAM Basque Center for Applied Mathematics, Bilbao, 2016. BCAM SpringerBriefs.

[15] T. L. Jackson and H. M. Byrne, *A mechanical model of tumor encapsulation and transcapsular spread*, vol. 180, 2002, pp. 307–328. John A. Jacquez memorial volume.

[16] A. Jüngel, *The boundedness-by-entropy method for cross-diffusion systems*, Nonlinearity, 28 (2015), pp. 1963–2001.

[17] A. Jungel and I. V. Stelzer, *Existence analysis of maxwell–stefan systems for multicomponent mixtures*, SIAM Journal on Mathematical Analysis, 45 (2013), pp. 2421–2440.

[18] A. Jüngel and A. Zurek, *A finite-volume scheme for a cross-diffusion model arising from interacting many-particle population systems*, in International Conference on Finite Volumes for Complex Applications, Springer, 2020, pp. 223–231.

[19] C. T. Kelley, *Iterative methods for linear and nonlinear equations*, vol. 16 of Frontiers in Applied Mathematics, Society for Industrial and Applied Mathematics (SIAM), Philadelphia, PA, 1995. With separately available software.

[20] ——, *Solving nonlinear equations with Newton's method*, vol. 1 of Fundamentals of Algorithms, Society for Industrial and Applied Mathematics (SIAM), Philadelphia, PA, 2003.

[21] K. Kergrene, L. Chamoin, M. Laforest, and S. Prudhomme, *On a goal-oriented version of the proper generalized decomposition method*, J. Sci. Comput., 81 (2019), pp. 92–111.

[22] K. Kunisch and S. Volkwein, *Control of the Burgers equation by a reduced-order approach using proper orthogonal decomposition*, J. Optim. Theory Appl., 102 (1999), pp. 345–371.

[23] ——, *Galerkin proper orthogonal decomposition methods for parabolic problems*, Numer. Math., 90 (2001), pp. 117–148.

[24] P. Ladevèze and L. Chamoin, *On the verification of model reduction methods based on the proper generalized decomposition*, Comput. Methods Appl. Mech. Engrg., 200 (2011), pp. 2032–2047.

[25] Y. Maday, *Reduced basis method for the rapid and reliable solution of partial differential equations*, in International Congress of Mathematicians. Vol. III, Eur. Math. Soc., Zürich, 2006, pp. 1255–1270.

[26] A. K. Noor and J. M. Peters, *Reduced basis technique for nonlinear analysis of structures*, AIAA Journal, 18 (1980), pp. 455–462.

[27] A. Nouy, *A priori model reduction through proper generalized decomposition for solving time-dependent partial differential equations*, Comput. Methods Appl. Mech. Engrg., 199 (2010), pp. 1603–1626.

[28] M. A. Olshanskii and E. E. Tyrtyshnikov, *Iterative methods for linear systems*, Society for Industrial and Applied Mathematics, Philadelphia, PA, 2014. Theory and applications.

[29] A. Quarteroni, A. Manzoni, and F. Negri, *Reduced basis methods for partial differential equations*, vol. 92 of Unitext, Springer, Cham, 2016. An introduction, La Matematica per il 3+2.

[30] Y. Saad, *Iterative methods for sparse linear systems*, Society for Industrial and Applied Mathematics, Philadelphia, PA, second ed., 2003.

[31] N. Shigesada, K. Kawasaki, and E. Teramoto, *Spatial segregation of interacting species*, J. Theoret. Biol., 79 (1979), pp. 83–99.

[32] N. Zamponi and A. Jüngel, *Analysis of degenerate cross-diffusion population models with volume filling*, in Annales de l'Institut Henri Poincaré C, Analyse non linéaire, vol. 34, Elsevier, 2017, pp. 1–29.